Cobalt based layered perovskites as cathode material for Intermediate Temperature Solid Oxide Fuel Cells: a brief review

Renato Pelosato[a*], *Giulio Cordaro*[a], *Davide Stucchi*[a], *Cinzia Cristiani*[a], *Giovanni Dotelli*[a]

[a] Politecnico di Milano, Dipartimento di Chimica Materiali e Ingegneria Chimica "G. Natta", Piazza Leonardo da Vinci 32, 20133 Milano, Italy

*corresponding author:

Renato Pelosato

Dipartimento di Chimica Materiali e Ingegneria Chimica "G. Natta"

Piazza Leonardo da Vinci 32, 20123 Milano (Italy)

Phone: 0039 02 2399 3232

Fax: 0039 02 7063 8173

e-mail: renato.pelosato@polimi.it

Abstract

Nowadays, the cathode is the most studied component in Intermediate Temperature-Solid Oxide Fuel Cells (IT-SOFCs). Decreasing SOFCs operating temperature implies slow oxygen reduction kinetics and large polarization losses. Double perovskites with general formula *RE*$BaCo_2O_{5+\delta}$ are promising mixed ionic-electronic conductors, offering a remarkable enhancement of the oxygen diffusivity and surface exchange respect to disordered perovskites. In this review, more than 250 compositions investigated in the literature were analyzed. The evaluation was performed in terms of electrical conductivity, Area Specific Resistance (ASR), chemical compatibility with electrolytes and Thermal Expansion Coefficient (TEC). The most promising materials have been identified as those bearing the mid-sized rare earths (Pr, Nd, Sm, Gd). Doping strategies have been analyzed: Sr doping on A site promotes higher electrical conductivity, but worsen ASR and TECs; B-site doping (Fe, Ni, Mn) helps lowering TECs, but is detrimental for the electrochemical properties. A promising boost of the electrochemical activity is obtained simply by introducing a slight Ba under-stoichiometry. Still, the high sensitivity of the electrochemical properties against slight changes in the stoichiometry hamper a conclusive comparison of all the investigated compounds. Opportunities for an improvement of double perovskite cathodes performance is tentatively foreseen in combining together the diverse effective doping strategies.

Keywords: solid oxide fuel cells; cathode; double perovskite; conductivity; ASR; doping.

1. Introduction.

Solid Oxide Fuel Cells (SOFCs) represent one of the most promising technology for clean energy production, because of a combination of high efficiency, high energy and power densities and fuel flexibility. SOFCs convert the chemical energy of a fuel into electrical energy through redox reactions. Large scale applications have been already developed in the last 50 years, such as on-board auxiliary power units, mobile power generators, and stationary power production. Decreasing SOFCs dimension would be of particular interest for powering long duration devices and remote communication electronics.

Conventional SOFCs must operate at high temperature (typically at ~1000 °C) to obtain the required performance. This high operating temperature leads to degradation of fuel cell elements, interfacial reactions among the components, and limits the choice of materials that can be used. Therefore, decreasing the operating temperature of SOFCs from the traditional ~1000 °C to an Intermediate Temperature (IT) range of 500-700 °C would reduce several drawbacks, such as short lifetime of the materials, high system and operating costs and limited material selection. One of the main advantages of decreasing operating temperature is the opportunity to use metallic interconnections inside the cell, instead of more expensive and brittle ceramic materials.

2. IT-SOFC Materials

2.1. Electrolyte

The most well-established part of IT-SOFC is the electrolyte, thanks to the extensive research carried out in the last years that led to encouraging outcomes for some of the investigated materials [1, 2]. Most of the research on electrolyte materials has been devoted to oxygen ion conductors (opposed to protonic conductors [3]), and Yttria-Stabilized Zirconia (YSZ) was first selected and extensively used in high temperature SOFCs; by the way, being the ionic conductivity a thermally activated process, lowering the operating temperature reduces the electrolyte performance. Therefore, alternative

materials are needed for operation in the intermediate temperature range. The most important requisite for an electrolyte material is a high ionic conductivity, in order to transfer O^{2-} ions towards anode section, and fluorite oxide (AO_2) compounds, such as YSZ, show good results only at high temperatures. An alternative electrolyte for IT-SOFC with fluorite structure is based on cerium oxide with addition of trivalent rare earths as dopants. The best performance has been achieved with gadolinium or samarium as dopants and the two compounds GDC ($Ce_{1-x}Gd_xO_2$) and SDC ($Ce_{1-x}Sm_xO_2$) are nowadays recognized as suitable intermediate temperature electrolytes. Another widely used material as electrolyte for IT-SOFCs is $La_{1-x}Sr_xGa_{1-y}Mg_yO_{3-(x+y)/2}$, generally referred to as LSGM. Although it exhibits high oxygen ion conductivity, LSGM is less used up to now than their fluorite counterparts, mainly because of many issues concerning the reactivity with the electrode materials and the difficulties in obtaining the material as a pure phase.

2.2. Anode

The anode is the part of the fuel cell where the fuel is oxidized and releases its electrons. Thus, anodic materials need to be both good catalysts for fuel oxidation and good electronic conductors to provide a path for the electrons to the external circuit. In addition, a Thermal Expansion Coefficient (TEC) value comparable to the electrolyte ones is required to maintain the layers adhesion and to guarantee a sufficient cell performance through several thermal cycles. Up to now, the most used anode material in SOFCs and IT-SOFCs is a composite of YSZ electrolyte and metallic nickel, known as cermet [4]. Although this cermet solved many problems, the Ni component has some weaknesses such as particle coarsening during operation and thermal expansion mismatch with YSZ; moreover, it promotes carbon deposition on the anode when the fuel cell is fed with hydrocarbon fuels. Hence, other cermets have been studied for anode, for example Cu-GDC, obtained by replacing nickel with copper and YSZ with doped cerium oxide ($Ce_{1-x}Gd_xO_2$). Recently, the use of perovskite materials in the anode side has raised some interest, in order to overcome the problems of redox stability of the cermets [5]. The most promising compounds are Cr based perovskites as $La_{0.75}Sr_{0.25}Cr_{0.5}Mn_{0.5}O_3$ (LSCM) [6] and

double perovskites based on strontium molybdates, such as Sr_2MnMoO_6 and Sr_2NiMoO_6 [7]. However, the activity of perovskites significantly drops at temperatures below 700 °C; therefore, this is still an open area of research for the improvement of cell performance.

2.3. Cathode

Nowadays, the cathode is the most studied component in IT-SOFCs. This happens because the cathodic reaction usually requires a very high activation energy; decreasing SOFCs operating temperature implies slower oxygen reduction reaction kinetics and therefore larger polarization losses; this causes a significant drop in fuel cell performance. Hence, extensive researches have been carried out on new cathodic materials, in order to improve cell efficiency in the intermediate temperature range. Since the conventional cathode for high temperature SOFCs is LSM ($La_xSr_{1-x}MnO_3$), similar perovskite materials have been widely studied. The first materials to be investigated were lanthanum manganite based perovskites, then cobaltite and ferrite based materials drew the attention of the scientific community and actually demonstrated better performance at lower temperature, thanks to their superior oxygen ion conductivity and higher stability. Also other solid oxides have been studied as alternative of simple perovskites, such as Ruddlesden-Popper series (RP) and double perovskites as examples [5].

RP oxides present general formula $A_{n+1}A'_2B_nO_{3n+1}$ and consist of $n$$ABO_3$ perovskite layers between two A'O rock-salt layers. In particular, materials with n = 1 exhibit a mixed ionic and electronic conductivity, appropriate electrochemical properties and suitable chemical and mechanical compatibilities with other SOFC components. This class of the RP family adopts the K_2NiF_4-type structure and results of particular interest for several solid electrolyte applications [8]. Among the materials with this structure, the RE_2MO_4 series (with *RE* = rare earths and M = transition metals) presents the best electrochemical performance [9].

Recently, double perovskites have become attractive structures for application in IT-SOFCs, demonstrating very good electrochemical performance for characteristic compositions. Their general formula can be written as $AA'B_2O_{5+\delta}$ and they are composed of alternate layers of single perovskite $ABO_{3-\delta}$ and $A'BO_{3-\delta}$; for this reason they are also termed 'layered perovskites'. Several manganite, cobaltite or ferrite based compounds can adopt the layered structure and indeed many composition have been prepared and characterized, using various dopants, in order investigate their chemical, electrochemical and thermal properties [10]. In particular, double perovskite materials in which a Rare Earth (*RE*) ion occupy the A site, barium the A' site and cobalt the B site, have received increasing consideration in recent years because of a combination of a high concentration of oxygen vacancies, a high electronic conductivity and excellent catalytic activity. Their general formula is reported as $REBaCo_2O_{5+\delta}$. However, there is still no obvious solution to the quest for optimized IT-SOFC cathode material.

For an exhaustive discussion of the general topic of cathode materials in SOFCs, the reader is referred to the reviews by Tsipis & Kharton [10-12]. In the next section of this review, the authors will give an overview of double perovskite compounds proposed for application in IT-SOFC cathodes.

3. Double (or Layered) Perovskites as cathodes: $AA'B_2O_{5+\delta}$

There is a general agreement in the scientific community that in order to maximize the performance in the intermediate temperature range, cathode materials need to hold mixed ionic-electronic conductivity properties, i.e. they shall be Mixed Ionic-Electronic Conductors, (MIECs). Since the Oxygen Reduction Reaction (ORR) is the step with highest activation energy, decreasing the operating temperature causes the largest electrical losses at the cathode. The reaction requires the direct contact of three different phases: gas (oxygen), electrode and electrolyte. This interface is called Three-Phase Boundary (TPB) and in traditional cathodes (i.e. pure electronic conductors) it is limited

to a thin region at the electrolyte surface, which extension is mainly determined by the morphologic structure of the cathode. MIECs instead, thanks to their oxygen ion conductivity, allow the diffusion of oxygen ions through the whole cathode layer; thus, this interface is extended to all the contact points between the gas and solid phase.

Among MIEC compounds, several perovskite and non-perovskite structures have been investigated. A few years ago, Tarancon and co-workers [13] published a review paper on *RE*$BaCo_2O_{5+\delta}$ MIEC compounds, summarizing the promising findings of the previous studies. Since then, an increasing interest has born about double perovskite materials, especially cobalt containing ones; particular efforts have been devoted to doping strategies, with the aim of improving the electric, electrochemical and thermal expansion characteristics of these compounds, in order to fit the requirements of IT-SOFC cathode materials. A considerable number of experimental and theoretical scientific papers have been published, reporting results concerning the synthesis and characterization of double perovskites for IT-SOFCs application. Starting from 2005, more than sixty publications reported a complete or partial electrochemical and thermal expansion characterization, providing useful information from a total of more than 250 compounds with different composition.

This increasing interest for double perovskite materials has been driven by the discovery that a perovskite structure offers a remarkable enhancement of the oxygen diffusivity when elements are ordered in alternate plan along *c* axis of the lattice. In fact, the regular layers of double perovskites reduce the oxygen bonding strength and produce channels for ion motion, providing a fast ionic conduction [14]. In order to obtain the desired regularly stacked structure, the choice of the composition of a double perovskite has to be properly made; the main driving force involved is the ionic radius of the elements that constitute the compound. It's fundamental that the difference between the ionic radii of the elements occupying A and A' site is significant, otherwise the two cations will randomly distribute in a disordered A(A')BO_3 lattice.

As mentioned above, rare earth elements (Sc, La, Ce, Pr, Nd, Pm, Sm, Eu, Gd, Y, Tb, Dy, Ho, Er, Tm, Yb, and Lu) usually occupy the A site in a typical double perovskite. Thus, for A' site is required an element with appropriate dimension; big ions, such as barium or strontium, have been used for this purpose. However, among all the investigated rare earths, a few gained most of the interest, and resulted to own the electrochemical and thermal properties suitable for application as IT-SOFC cathodes.

Transition metals are situated in the B site and can be found alone or in various mixed compositions with other elements. The most used ones are cobalt, manganese, iron and copper; Co based double perovskites (*RE*$BaCo_2O_{5+\delta}$) usually offer the highest catalytic activity for the oxygen reduction reaction [15-17]. In fact, this class of compounds can accept a wide range of oxygen concentrations ($5 \leq 5+\delta \leq 6$), driven by the mean Co oxidation state; the oxygen content in the final material has also a correlation with the size of the A and A' cations and furthermore it can also be governed by the annealing conditions. A linear relationship has been reported between the oxygen content and A site ionic radii difference [r(A)-r(A')] by some authors [17]. As the size of the A cation decreases, the mean oxygen content at room temperature decreases, according to Anderson et al. and Maignan et al. [18, 19] from nearly 6 for $LaBaCo_2O_{5+\delta}$, about 5.7 for $PrBaCo_2O_{5+\delta}$ and $NdBaCo_2O_{5+\delta}$, between 5.5 and 5.4 for $YBaCo_2O_{5+\delta}$, $SmBaCo_2O_{5+\delta}$, $EuBaCo_2O_{5+\delta}$, $GdBaCo_2O_{5+\delta}$ and $TbBaCo_2O_{5+\delta}$, down to approximately 5.3 for $DyBaCo_2O_{5+\delta}$ and $HoBaCo_2O_{5+\delta}$ when annealed in air[18, 19]. According to the data collected in this review, the reported values for the undoped compounds are: 5.80÷6.00 for $LaBaCo_2O_{5+\delta}$, 5.64÷5.89 for $PrBaCo_2O_{5+\delta}$, 5.62÷5.85 for $NdBaCo_2O_{5+\delta}$, between 5.31÷5.51 for $YBaCo_2O_{5+\delta}$, 5.40÷5.69 $SmBaCo_2O_{5+\delta}$, 5.40÷5.66 for $GdBaCo_2O_{5+\delta}$, 5.40÷5.52 $EuBaCo_2O_{5+\delta}$, and 5.40 $TbBaCo_2O_{5+\delta}$, and down to approximately 5.30÷5.36 for $DyBaCo_2O_{5+\delta}$ and 5.14÷5.30 $HoBaCo_2O_{5+\delta}$. These values can also vary depending on the treatment atmosphere and the preparation procedure. The relative ionic radii of the two A site cations even drives structural transitions in these compounds. According to Kim and Manthiram [20], is possible that a disordered structure is obtained

with large rare earth ions, such as La, because too similar ionic dimension to Ba cation. Thus, La-based perovskites can be considered as doped simple perovskite with general formula $A_{0.5}A'_{0.5}BO_3$, confirmed by the fact that La-based compounds can be usually indexed with a cubic lattice.

In addition, the unit cell volume increases with rare earths dimension, and, in order to maintain a regular structure, Co ions are driven to adopt the electronic configuration that minimizes their ionic size [20]. Since increasing the oxidation state from Co^{3+} to Co^{4+}, the Co ionic radius decreases, this causes in La-based perovskites the tendency to an average oxidation state of Co near to 3.5 and hence an oxygen content equivalent to about 6 moles per mole of compound. These parameters reveal a lack of induced oxygen vacancies in the lattice, that causes a very low ionic conductivity, hence a reduced oxygen reduction kinetic. Nonetheless, the ordered structure has been also achieved in lanthanum compounds by some authors by carefully tailoring the annealing temperatures, rates and atmosphere, as in the case of Rautama et al. [21]. Still, the main issue in La-based perovskites is the very high TEC value, caused by elevated ionicity of the La-O bonds. Kim and Manthiram [20] reported a TEC equal to 24.3 10^6 K^{-1} for the $LaBaCo_2O_{5+\delta}$ compound.

At the opposite side, when the size difference between Ba and *RE* cation is high, the ordered structure can be easily obtained. On the other hand, this usually leads to a reduction of the electrical conductivity, attributed to the very high concentration of oxygen vacancies that is supposed to cause a distortion of the O-Co-O bonds, hampering the conduction mechanism [22]. Moreover, compounds like $YBaCo_2O_{5+\delta}$ and $HoBaCo_2O_{5+\delta}$ (that have the largest size difference with barium) are sensitive to decomposition in air atmosphere at high temperatures [23]; those compounds can be stabilized only by releasing the size difference with proper doping [24]. However, several publications focused their attention on these rare earths in A site, trying to improve catalytic activity and chemical stability with the addition of dopants elements [24, 25], because those small rare earths usually allow obtaining the lowest TEC values among $REBaCo_2O_{5+\delta}$ series [20].

The most common crystal structure obtained for double perovskite compounds is Tetragonal (commonly space group *P4/mmm*). However, many papers report an enhanced distortion of the lattice structure that leads to Orthorhombic one (typically *Pmmm*). This slight structural change has been related to rare earth ionic dimension, hence to the oxygen content of the material [18, 20]. Anderson et al. [18] tried to demonstrate that oxygen content is the fundamental parameter for the structure arrangement of the *RE*$BaCo_2O_{5+\delta}$ series. Varying the oxygen content in the $NdBaCo_2O_{5+\delta}$ compound, by using a controlled atmosphere during the synthesis, allowed the production of the same material with different crystal structures. Although $NdBaCo_2O_{5+\delta}$ usually presents a tetragonal structure, compounds with oxygen content between 5.25 and 5.6 adopted an orthorhombic arrangement. However, has been shown that even thermal treatments can control the lattice structure of the materials, despite similar oxygen contents. The *RE*$BaCo_2O_{5+\delta}$ series (*RE* = Pr, Nd, Sm and Gd) synthesized by Chavez et al. [26] revealed how cooling rate plays a dominant role, because at high temperature these compounds change their crystal structure and then retain it with a sufficiently fast cooling. Also, other publications reported that is possible to obtain $GdBaCo_2O_{5+\delta}$ [27] and $YBaCo_2O_{5+\delta}$ [28] with either tetragonal or orthorhombic lattice by controlling the synthesis conditions.

In the following sections, the authors will mainly focus on a few electrochemical and thermal parameters to compare the investigated cathode materials: total electrical conductivity, area specific resistance (ASR) and thermal expansion coefficient (TEC). However, also oxygen content, lattice cell parameters, synthesis method, and other available data have been collected and reported in order to give a thorough point of view of the characteristics of different layered perovskite compounds. The papers included into this process are those that report experimental results about synthesis of a cobalt based double perovskite along with a complete - or at least partial - electrochemical characterization. The focus will be then limited to the most promising ones (in Section 4), and on the outcomes of the different doping strategies on their electrical, electrochemical and thermal characteristics (Section 5).

3.1. General overview

A huge amount of papers have been published recently dealing with the synthesis and characterization of double perovskites for cathode application. These papers have been collected and the results obtained by the scientific community have been summarized. The relevant physical, chemical and electrochemical parameters are reported in the following tables for several compounds. The same compound can appear several times in the tables if it was investigated by different researchers or synthesized with different preparation techniques.

In the following tables, the total electric conductivity [$S \cdot cm^{-1}$] and the ASR [$\Omega \cdot cm^2$] measured in symmetric cells are reported for each compound at 600 and 700 °C; thermal expansion coefficients [10^6 K^{-1}] are reported for the widest available temperature interval, usually comprising measurements from 20-100 to 800-1000 °C, depending on the paper. The relevant chemical and physical parameters like preparation method, sintering temperature, lattice type and cell parameters, oxygen content are also reported for the same compounds. Synthesis methods most frequently found in literature are the traditional solid state reaction (referred to as SS), direct combustion method (C), sol-gel technique (SG) mainly using Ethylenediaminetetraacetic-Acid and citrates as gelling agents, or the classic pechini method (P) using citric acid and ethylene glycol. The crystal lattice is reported for each composition when the X-Ray diffraction data were indexed by the authors, and all the compounds adopted either a tetragonal (T), orthorhombic (O) or cubic (C) lattice.

Table 1 reports some selected electrochemical and thermal parameters of La-based compounds; table 2 reports other relevant chemical and physical parameters and the preparation method and temperature for the same compounds.

Table 1. Composition, electrical conductivity σ, ASR and TEC of La-based double perovskite cathodes

COMPOSITION	σ @ 600 °C [S·cm^{-1}]	σ @ 700 °C [S·cm^{-1}]	ASR @ 600 °C [Ω·cm^2]	ASR @ 700 °C [Ω·cm^2]	E att [eV]	TEC [10^6 K^{-1}]	Reference
$LaBaCo_2O_{5+\delta}$	1443	1076	-	-	-	24.3	**[20]**
$LaBaCo_2O_{5+\delta}$	60.0	52.2	3.56	0.56	-	-	**[29]**
$LaBaCo_2O_{5+\delta}$	459	457	-	-	-	-	**[30]**
$LaBaCuCoO_{5+\delta}$	392	345	-	-	-	-	**[31]**
$LaBaCuFeO_{5+\delta}$	123	93.7	-	-	-	-	**[31]**
$LaSrMnCoO_{5+\delta}$	111	124	-	-	-	15.8	**[32]**

Table 2. Composition, synthetic route, sintering temperature, lattice type and parameters and oxygen content of La-based double perovskite cathodes. SS = Solid state; SG = Sol-Gel; C = Combustion; P = Pechini

COMPOSITION	Synthesis Method	Sintering Temp [°C]	Lattice type	*a* [Å]	*b* [Å]	*c* [Å]	Oxygen content [5+δ]	Reference
$LaBaCo_2O_{5+\delta}$	SS	1100	C	3.940	-	-	6.00	**[33]**
$LaBaCo_2O_{5+\delta}$	SS	1100	C	3.881	-	-	6.00	**[20]**
$LaBaCo_2O_{5+\delta}$	SG	1150	O	3.898	3.891	7.718	5.80	**[29]**

In La-Based compounds, the highest electrical conductivity is obtained in the disordered compound with the cubic structure (Table 1 and 2, ref. [20]), while for La-based ordered perovskites much lower values are reported, sharply enhanced only in the Cu-doped compounds ([31]). ASR measurements are available only in the work by Zhang et al [29] and are quite high respect to other compounds

reported below, despite the evidence of the ordered structure and the presence of oxygen vacancies (oxygen content = 5.80, Table 2, ref. [29]).

Table 3 reports some selected electrochemical and thermal parameters of Pr-based compounds; table 4 reports other relevant chemical and physical parameters and the preparation method and temperature for the same compounds.

Table 3. Composition, electrical conductivity σ, ASR and TEC of Pr-based double perovskite cathodes

COMPOSITION	**σ @ 600 °C [S·cm^{-1}]**	**σ @ 700 °C [S·cm^{-1}]**	**ASR @ 600 °C [Ω·cm^2]**	**ASR @ 700 °C [Ω·cm^2]**	**E att [eV]**	**TEC [10^6 K^{-1}]**	**Reference**
$PrBaCo_2O_{5+\delta}$	-	-	-	-	0.95	21.5	**[34]**
$PrBaCo_2O_{5+\delta}$	894	730	-	-	-	-	**[35]**
$PrBaCo_2O_{5+\delta}$	-	-	-	-	-	21.5	**[36]**
$PrBaCo_2O_{5+\delta}$	844	695	-	0.75	-	20.4	**[37]**
$PrBaCo_2O_{5+\delta}$	-	-	0.18	0.04	1.19	-	**[38]**
$PrBaCo_2O_{5+\delta}$	-	-	13.2	0.67	-	-	**[26]**
$PrBaCo_2O_{5+\delta}$	161	141	0.21	0.02	-	24.1	**[29]**
$PrBaCo_2O_{5+\delta}$	214	172	-	-	-	24.6	**[39]**
$PrBaCo_2O_{5+\delta}$	-	-	1.83	0.21	-	-	**[40]**
$PrBaCo_2O_{5+\delta}$	392	364	0.87	0.18	-	-	**[41]**
$PrBaCo_2O_{5+\delta}$	588	437	0.12	-	-	-	**[42]**
$PrBaCoCuO_{5+\delta}$	144	124	0.21	0.05	-	15.2	**[43]**
$PrBaCoFeO_{5+\delta}$	204	163	-	-	-	21.0	**[44]**
$PrBaCoFeO_{5+\delta}$	-	-	-	-	-	21.0	**[44]**

$PrBaCoFeO_{5+\delta}$	-	-	-	-	-	21.0	**[34]**
$PrBaCoFeO_{5+\delta}$	72.8	65.3	1.69	0.28	-	-	**[41]**
$PrBaFe_2O_{5+\delta}$	9.2	7.1	-	-	-	17.2	**[39]**
$PrBaFe_2O_{5+\delta}$	25.4	22.7	2.76	0.48	-	-	**[41]**
$PrSrCo_2O_{5+\delta}$	2084	1776	0.19	-	0.93	-	**[42]**
$PrBaCo_{1.0}Fe_{1.0}O_{5+\delta}$	91.8	68.4	-	-	-	25.0	**[39]**
$Pr_{0.3}Y_{0.7}BaCo_2O_{5+\delta}$	414	420	1.25	0.18	-	-	**[36]**
$Pr_{0.5}Y_{0.5}BaCo_2O_{5+\delta}$	582	564	1.46	0.20	-	17.2	**[36]**
$Pr_{0.7}Y_{0.3}BaCo_2O_{5+\delta}$	730	649	0.90	0.12	-	17.6	**[36]**
$PrBa_{0.5}Sr_{0.5}Co_2O_{5+\delta}$	-	-	0.08	0.02	-	-	**[45]**
$PrBa_{0.5}Sr_{0.5}Co_2O_{5+\delta}$	998	818	-	0.09	-	-	**[46]**
$PrBa_{0.5}Sr_{0.5}Co_2O_{5+\delta}$	998	818	-	0.19	-	-	**[46]**
$PrBa_{0.5}Sr_{0.5}Co_2O_{5+\delta}$	-	-	0.85	0.44	1.23	-	**[47]**
$PrBa_{0.5}Sr_{0.5}Co_2O_{5+\delta}$	492	395	0.85	0.44	1.07	-	**[48]**
$PrBa_{0.5}Sr_{0.5}Co_2O_{5+\delta}$	1240	981	0.07	-	-	-	**[42]**
$PrBa_{0.5}Sr_{0.5}CoFeO_{5+\delta}$	-	-	0.11	0.02	-	-	**[45]**
$PrBa_{0.5}Sr_{0.5}CoFeO_{5+\delta}$	342	260	-	-	-	20.9	**[49]**
$PrBaCo_{0.5}Fe_{1.5}O_{5+\delta}$	10.2	7.1	-	-	-	19.1	**[39]**
$PrBaCo_{1.2}Fe_{0.8}O_{5+\delta}$	110	103	1.49	0.29	-	-	**[41]**
$PrBaCo_{1.4}Fe_{0.6}O_{5+\delta}$	330	303	1.13	0.20	-	-	**[41]**
$PrBaCo_{1.5}Fe_{0.5}O_{5+\delta}$	132	104	-	-	-	26.0	**[39]**
$PrBaCo_{1.6}Fe_{0.4}O_{5+\delta}$	404	382	0.50	0.13	-	-	**[41]**
$PrBaCo_{1.6}Ni_{0.4}O_{5+\delta}$	748	620	-	-	-	16.6	**[50]**
$PrBaCo_{1.8}Fe_{0.2}O_{5+\delta}$	194	170	1.08	0.20	-	-	**[41]**
$PrBa_{0.5}Sr_{0.5}Co_{0.5}Fe_{1.5}O_{5+\delta}$	128	95.5	-	-	-	19.2	**[49]**
$PrBa_{0.5}Sr_{0.5}Co_{1.5}Fe_{0.5}O_{5+\delta}$	-	-	0.06	0.02	-	-	**[45]**
$PrBa_{0.5}Sr_{0.5}Co_{1.5}Fe_{0.5}O_{5+\delta}$	422	337	-	-	-	21.3	**[49]**
$PrBa_{0.5}Sr_{0.5}Co_{1.7}Ni_{0.3}O_{5+\delta}$	903	646	13.3	1.75	-	19.7	**[51]**
$PrBa_{0.5}Sr_{0.5}Co_{1.8}Ni_{0.2}O_{5+\delta}$	835	640	12.4	1.63	-	20.6	**[51]**
$PrBa_{0.5}Sr_{0.5}Co_{1.9}Ni_{0.1}O_{5+\delta}$	938	771	8.56	1.64	-	21.9	**[51]**

$PrBaCo_{1.50}Sc_{0.5}O_{5+\delta}$	208	171	0.12	0.03	0.91	19.9	**[38]**
$PrBaCo_{1.80}Sc_{0.2}O_{5+\delta}$	165	136	0.15	0.03	1.06	22.8	**[38]**
$PrBaCo_{1.90}Sc_{0.1}O_{5+\delta}$	101	84.4	0.15	0.04	1.07	23.0	**[38]**
$Pr_{1.05}Ba_{0.95}Co_2O_{5+\delta}$	847	700	-	0.32	-	21.6	**[37]**
$Pr_{1.10}Ba_{0.90}Co_2O_{5+\delta}$	893	736	-	0.13	-	21.8	**[37]**
$Pr_{1.20}Ba_{0.80}Co_2O_{5+\delta}$	849	710	-	0.23	-	18.8	**[37]**
$Pr_{1.30}Ba_{0.70}Co_2O_{5+\delta}$	789	676	-	0.30	-	18.4	**[37]**
$PrBa_{0.25}Sr_{0.75}Co_2O_{5+\delta}$	1824	1625	0.08	-	-	-	**[42]**
$PrBa_{0.75}Sr_{0.25}Co_2O_{5+\delta}$	1020	813	0.10	-	-	-	**[42]**
$PrBaCo_{1.95}Sc_{0.05}O_{5+\delta}$	15.8	13.8	0.16	0.04	1.15	23.6	**[38]**
$PrBaCo_{0.66}Fe_{0.66}Cu_{0.66}O_{5+\delta}$	144	131	-	0.55	-	16.6	**[34]**

Table 4. Composition, synthetic route, sintering temperature, lattice type and parameters and oxygen content of Pr-based double perovskite cathodes.

COMPOSITION	**Synthesis Method**	**Sintering Temp [°C]**	**Lattice type**	***a* [Å]**	***b* [Å]**	***c* [Å]**	**Oxygen content [5+δ]**	**Reference**
$PrBaCo_2O_{5+\delta}$	SS	1100	-	-	-	-	5.68	**[18]**
$PrBaCo_2O_{5+\delta}$	C	950	O	3.868	3.871	7.576	5.79	**[39]**
$PrBaCo_2O_{5+\delta}$	P	1100	O	3.915	3.902	7.699	5.78	**[42]**
$PrBaCo_2O_{5+\delta}$	SG	1150	O	3.896	3.890	7.612	5.77	**[29]**
$PrBaCo_2O_{5+\delta}$	SG	1000	T	3.909	-	7.638	5.64	**[37]**
$PrBaCo_2O_{5+\delta}$	SG	950	T	3.894	-	7.636	-	**[41]**
$PrBaCo_2O_{5+\delta}$	SS	1100	T	3.946	-	7.610	5.89	**[33]**
$PrBaCo_2O_{5+\delta}$	SS	1100	T*	3.902	3.906	7.631	5.70	**[19]**
$PrBaCoFeO_{5+\delta}$	SG	950	C	3.899	-	-	-	**[41]**
$PrBaCoFeO_{5+\delta}$	SG	1150	T	3.918	-	7.657	5.79	**[44]**
$PrBaFe_2O_{5+\delta}$	SG	950	C	3.947	-	-	-	**[41]**
$PrBaFe_2O_{5+\delta}$	C	950	O	3.928	3.934	7.794	5.88	**[39]**

$PrSrCo_2O_{5+\delta}$	P	1100	O	5.437	5.403	7.642	6.00	**[42]**
$PrBaCo_{1.0}Fe_{1.0}O_{5+\delta}$	C	950	O	3.893	3.898	7.681	5.82	**[39]**
$Pr_{0.3}Y_{0.7}BaCo_2O_{5+\delta}$	SS	1000	T	-	-	-	5.29	**[36]**
$Pr_{0.5}Y_{0.5}BaCo_2O_{5+\delta}$	SS	1000	T	-	-	-	5.42	**[36]**
$Pr_{0.7}Y_{0.3}BaCo_2O_{5+\delta}$	SS	1000	T	-	-	-	5.49	**[36]**
$PrBa_{0.5}Sr_{0.5}Co_2O_{5+\delta}$	P	1100	T	3.869	-	7.732	5.84	**[42]**
$PrBa_{0.5}Sr_{0.5}Co_2O_{5+\delta}$	SS	1000	T	3.855	-	7.729	5.50	**[48]**
$PrBa_{0.5}Sr_{0.5}CoFeO_{5+\delta}$	SG	1000	O	3.865	3.864	7.727	5.76	**[49]**
$PrBaCo_{0.5}Fe_{1.5}O_{5+\delta}$	C	950	O	3.913	3.917	7.766	5.88	**[39]**
$PrBaCo_{1.2}Fe_{0.8}O_{5+\delta}$	SG	950	C	3.895	-	-	-	**[41]**
$PrBaCo_{1.4}Fe_{0.6}O_{5+\delta}$	SG	950	C	3.882	-	-	-	**[41]**
$PrBaCo_{1.5}Fe_{0.5}O_{5+\delta}$	C	950	O	3.875	3.879	7.611	5.81	**[39]**
$PrBaCo_{1.6}Fe_{0.4}O_{5+\delta}$	SG	950	C	3.879	-	-	-	**[41]**
$PrBaCo_{1.6}Ni_{0.4}O_{5+\delta}$	SG	1200	T	3.908	-	7.638	-	**[50]**
$PrBaCo_{1.8}Fe_{0.2}O_{5+\delta}$	SG	950	T	3.889	-	7.661	-	**[41]**
$PrBa_{0.5}Sr_{0.5}Co_{0.5}Fe_{1.5}O_{5+\delta}$	SG	1000	O	3.883	3.884	7.765	5.82	**[49]**
$PrBa_{0.5}Sr_{0.5}Co_{1.5}Fe_{0.5}O_{5+\delta}$	SG	1000	O	3.851	3.854	7.715	5.67	**[49]**
$PrBa_{0.5}Sr_{0.5}Co_{1.7}Ni_{0.3}O_{5+\delta}$	SG	1100	O	3.884	3.860	7.672	-	**[51]**
$PrBa_{0.5}Sr_{0.5}Co_{1.8}Ni_{0.2}O_{5+\delta}$	SG	1100	O	3.908	3.859	7.612	-	**[51]**
$PrBa_{0.5}Sr_{0.5}Co_{1.9}Ni_{0.1}O_{5+\delta}$	SG	1100	O	3.863	3.852	7.707	-	**[51]**
$PrBaCo_{1.50}Sc_{0.5}O_{5+\delta}$	SG	1050	C	-	-	-	5.64	**[38]**
$PrBaCo_{1.80}Sc_{0.2}O_{5+\delta}$	SG	1050	T	-	-	-	5.71	**[38]**
$PrBaCo_{1.90}Sc_{0.1}O_{5+\delta}$	SG	1050	T	-	-	-	5.72	**[38]**
$Pr_{1.05}Ba_{0.95}Co_2O_{5+\delta}$	SG	1000	T	3.899	-	7.632	5.65	**[37]**
$Pr_{1.10}Ba_{0.90}Co_2O_{5+\delta}$	SG	1000	T	3.891	-	7.619	5.70	**[37]**
$Pr_{1.20}Ba_{0.80}Co_2O_{5+\delta}$	SG	1000	T	3.878	-	7.620	5.77	**[37]**
$Pr_{1.30}Ba_{0.70}Co_2O_{5+\delta}$	SG	1000	T	3.870	-	7.624	5.83	**[37]**
$PrBa_{0.25}Sr_{0.75}Co_2O_{5+\delta}$	P	1100	T	3.842	-	7.677	5.90	**[42]**
$PrBa_{0.75}Sr_{0.25}Co_2O_{5+\delta}$	P	1100	O	3.897	3.879	7.682	5.79	**[42]**
$PrBaCo_{1.95}Sc_{0.05}O_{5+\delta}$	SG	1050	T	-	-	-	5.74	**[38]**

$PrBaCo_{0.66}Fe_{0.66}Cu_{0.66}O_{5+\delta}$	SG	950	T	3.904	-	7.651	-	**[34]**

* tetragonal with orthorhombic superstructure

It is quite challenging to draw conclusions comparing Pr-based componds properties; a lot of efforts have been devoted to synthesize and characterize those compounds, with doping in either A and B sublattices, and very diverse results have been obtained. Generally, electrical conductivity values are the highest among the series and the ASR are the lowest, except for those compounds doped with iron or scandium on cobalt site (Table 3). Also many of the compounds bearing iron or scandium are found to adopt a cubic structure, as if those elements promote an ordering of the lattice. The reported oxygen contents spread in the 5.29 ÷6.00 range, even if the lowest values are obtained when Pr is partially substituted by Y ([36]). Thermal expansion coefficients of these compounds can range from 15.2 [10^6 K^{-1}] ([43] for Cu doped compound) up to 26 [10^6 K^{-1}] ([39]) but mainly show values around 20 [10^6 K^{-1}].

Table 5 reports some selected electrochemical and thermal parameters of Nd-based compounds; table 6 reports other relevant chemical and physical parameters and the preparation method and temperature for the same compounds.

Table 5. Composition, electrical conductivity σ, ASR and TEC of Nd-based double perovskite cathodes

COMPOSITION	**σ @ 600 °C [$S \cdot cm^{-1}$]**	**σ @ 700 °C [$S \cdot cm^{-1}$]**	**ASR @ 600 °C [$\Omega \cdot cm^2$]**	**ASR @ 700 °C [$\Omega \cdot cm^2$]**	**E att [eV]**	**TEC [10^6 K^{-1}]**	**Reference**
$NdBaCo_2O_{5+\delta}$	-	-	0.58	0.11	1.19	22.3	**[52]**
$NdBaCo_2O_{5+\delta}$	-	-	-	-	-	23.1	**[53]**

$NdBaCo_2O_{5+\delta}$	952	740	-	-	-	19.1	**[20]**
$NdBaCo_2O_{5+\delta}$	-	-	-	-	-	23.1	**[54]**
$NdBaCo_2O_{5+\delta}$	-	-	5.59	0.30	-	-	**[26]**
$NdBaCo_2O_{5+\delta}$	192	168	0.28	0.04	-	-	**[29]**
$NdBaCo_2O_{5+\delta}$	-	-	4.52	1.18	-	-	**[40]**
$NdBaCo_2O_{5+\delta}$	448	343	0.18	0.04	-	-	**[55]**
$NdBaCo_2O_{5+\delta}$	776	633	1.93	0.70	1.68	21.5	**[56]**
$NdBaCoCuO_{5+\delta}$	95.1	99.2	1.51	0.28	-	16.9	**[57]**
$NdBaCoFeO_{5+\delta}$	116	96.8	-	-	-	19.5	**[44]**
$NdBaCoFeO_{5+\delta}$	70.6	59.2	-	-	-	19.5	**[44]**
$NdBaCoFeO_{5+\delta}$	102	85.6	2.48	0.90	1.71	20.0	**[56]**
$NdBaFe_2O_{5+\delta}$	11.7	9.5	-	-	1.08	18.3	**[56]**
$NdSrCo_2O_{5+\delta}$	2420	2169	0.27	0.05	-	-	**[55]**
$NdBa_{0.5}Sr_{0.5}Co_2O_{5+\delta}$	-	-	1.17	0.25	1.34	24.3	**[52]**
$NdBa_{0.5}Sr_{0.5}Co_2O_{5+\delta}$	2412	2100	0.11	-	-	20.3	**[58]**
$NdBa_{0.5}Sr_{0.5}Co_2O_{5+\delta}$	255	204	1.06	0.55	1.34	-	**[48]**
$NdBa_{0.5}Sr_{0.5}CoCuO_{5+\delta}$	261	227	3.77	0.52	-	18.9	**[57]**
$NdBaCo_{0.5}Fe_{1.5}O_{5+\delta}$	39.2	31.2	3.66	1.23	1.80	20.7	**[56]**
$NdBaCo_{1.5}Fe_{0.5}O_{5+\delta}$	473	392	1.32	0.54	1.45	20.8	**[56]**
$NdBaCo_{1.6}Ni_{0.4}O_{5+\delta}$	654	521	-	-	1.22	19.4	**[50]**
$NdBa_{0.5}Sr_{0.5}Co_{1.5}Mn_{0.5}O_{5+\delta}$	717	665	0.16	-	-	14.3	**[58]**
$NdBa_{0.25}Sr_{0.75}Co_2O_{5+\delta}$	2082	1546	0.13	0.03	1.32	-	**[55]**
$NdBa_{0.25}Sr_{0.75}CoCuO_{5+\delta}$	211	185	1.25	0.21	-	17.0	**[57]**
$NdBa_{0.50}Sr_{0.50}Co_2O_{5+\delta}$	1501	1102	0.12	0.03	-	-	**[55]**
$NdBa_{0.75}Sr_{0.25}Co_2O_{5+\delta}$	550	461	0.17	0.03	-	-	**[55]**
$NdBa_{0.75}Sr_{0.25}CoCuO_{5+\delta}$	143	123	1.68	0.33	-	18.5	**[57]**
$NdBa_{0.5}Sr_{0.5}Co_{1.75}Mn_{0.25}O_{5+\delta}$	1133	1004	0.13	-	-	16.4	**[58]**
$NdBaCo_{0.66}Fe_{0.66}Cu_{0.66}O_{5+\delta}$	91.8	88.0	1.14	0.21	-	-	**[59]**
$NdBaCo_{0.66}Fe_{0.66}Cu_{0.66}O_{5+\delta}$	91.8	88.0	0.60	0.08	-	-	**[59]**

Table 6. Composition, synthetic route, sintering temperature, lattice type and parameters and oxygen content of Nd-based double perovskite cathodes.

COMPOSITION	Synthesis Method	Sintering Temp [°C]	Lattice type	*a* [Å]	*b* [Å]	*c* [Å]	Oxygen content [5+δ]	Reference
$NdBaCo_2O_{5+\delta}$	SS	1100	T	3.903	-	7.614	5.73	**[53]**
$NdBaCo_2O_{5+\delta}$	SS	1100	T	3.939	-	7.576	5.85	**[33]**
$NdBaCo_2O_{5+\delta}$	SS	1100	T	3.895	-	7.611	5.78	**[20]**
$NdBaCo_2O_{5+\delta}$	SS	1100	T	3.903	-	7.614	5.73	**[54]**
$NdBaCo_2O_{5+\delta}$	SS	1100	T*	3.897	3.902	7.612	5.70	**[19]**
$NdBaCo_2O_{5+\delta}$	SS	1100	-	-	-	-	5.62	**[18]**
$NdBaCo_2O_{5+\delta}$	SG	1150	O	3.872	3.889	7.599	5.69	**[29]**
$NdBaCo_2O_{5+\delta}$	P	1100	O	3.918	3.909	7.635	5.78	**[55]**
$NdBaCo_2O_{5+\delta}$	SS	1100	T	3.896	-	7.619	5.85	**[56]**
$NdBaCoCuO_{5+\delta}$	SS	1000	T	3.920	-	7.683	5.78	**[57]**
$NdBaCoFeO_{5+\delta}$	SG	1150	T	3.909	-	7.625	5.67	**[44]**
$NdBaCoFeO_{5+\delta}$	SS	1100	T	3.912	-	7.704	6.00	**[56]**
$NdBaFe_2O_{5+\delta}$	SS	1100	C	3.930	-	-	6.00	**[56]**
$NdSrCo_2O_{5+\delta}$	P	1100	O	5.374	5.420	7.602	6.00	**[55]**
$NdBa_{0.5}Sr_{0.5}Co_2O_{5+\delta}$	P	1000	T	3.894	-	7.615	5.88	**[58]**
$NdBa_{0.5}Sr_{0.5}Co_2O_{5+\delta}$	SS	1000	T	3.849	-	7.725	5.23	**[48]**
$NdBa_{0.5}Sr_{0.5}CoCuO_{5+\delta}$	SS	1000	T	3.871	-	7.664	5.79	**[57]**
$NdBaCo_{0.5}Fe_{1.5}O_{5+\delta}$	SS	1100	C	3.912	-	-	6.00	**[56]**
$NdBaCo_{1.5}Fe_{0.5}O_{5+\delta}$	SS	1100	T	3.905	-	7.661	6.00	**[56]**

$NdBaCo_{1.6}Ni_{0.4}O_{5+\delta}$	SG	1200	T	3.902	-	7.620	-	**[50]**
$NdBa_{0.5}Sr_{0.5}Co_{1.5}Mn_{0.5}O_{5+\delta}$	P	1000	T	3.856	-	7.705	5.83	**[58]**
$NdBa_{0.25}Sr_{0.75}Co_2O_{5+\delta}$	P	1100	T	3.895	-	7.610	5.89	**[55]**
$NdBa_{0.25}Sr_{0.75}CoCuO_{5+\delta}$	SS	1000	T	3.894	-	7.667	5.69	**[57]**
$NdBa_{0.50}Sr_{0.50}Co_2O_{5+\delta}$	P	1100	T	3.894	-	7.615	5.89	**[55]**
$NdBa_{0.75}Sr_{0.25}Co_2O_{5+\delta}$	P	1100	O	3.896	3.883	7.646	5.78	**[55]**
$NdBa_{0.75}Sr_{0.25}CoCuO_{5+\delta}$	SS	1000	T	3.900	-	7.672	5.75	**[57]**
$NdBa_{0.5}Sr_{0.5}Co_{1.75}Mn_{0.25}O_{5+\delta}$	P	1000	T	3.858	-	7.713	5.78	**[58]**
$NdBaCo_{0.66}Fe_{0.66}Cu_{0.66}O_{5+\delta}$	SG	1400	T	3.923	-	7.696	5.44	**[59]**
$NdBaCo_{0.66}Fe_{0.66}Cu_{0.66}O_{5+\delta}$	SG	1400	T	3.923	-	7.696	5.44	**[59]**

* tetragonal with orthorhombic superstructure

Also in the case of Nd-based compounds, it is worth noting the large spread of measured electrical conductivity values (see Table 5, ref [20] and [29] for an example regarding the undoped compounds). Very high values are often reported for Sr-doped compounds. As for Pr-based compounds, iron doping seem to promote a change of the structure towards a disordered cubic with higher oxygen contents (see for example ref. [56]). ASR as low as 0.04 $\Omega \cdot cm^2$ are reported at 700 °C (Table 5, [29], [55]) for the undoped compound, probably as a result of the very effective oxygen surface exchange ability of Nd-based compounds [60]. Oxygen content ranges between 5.62 ÷ 5.85 for $NdBaCo_2O_{5+\delta}$ and extends to 5.23 ÷ 6.00 for all the reported compounds.

Table 7 reports some selected electrochemical and thermal parameters of Sm-based compounds; table 8 reports other relevant chemical and physical parameters and the preparation method and temperature for the same compounds.

Table 7. Composition, electrical conductivity σ, ASR and TEC of Sm-based double perovskite cathodes

COMPOSITION	σ @ 600 °C [S·cm^{-1}]	σ @ 700 °C [S·cm^{-1}]	ASR @ 600 °C [Ω·cm^2]	ASR @ 700 °C [Ω·cm^2]	E att [eV]	TEC [10^6 K^{-1}]	Reference
$SmBaCo_2O_{5+\delta}$	-	-	-	-	-	21.2	[53]
$SmBaCo_2O_{5+\delta}$	836	633	-	-	-	17.1	[20]
$SmBaCo_2O_{5+\delta}$	556	443	0.19	-	-	-	[61]
$SmBaCo_2O_{5+\delta}$	-	-	-	-	-	20.8	[54]
$SmBaCo_2O_{5+\delta}$	-	-	16.5	1.53	-	-	[26]
$SmBaCo_2O_{5+\delta}$	226	193	0.54	0.09	-	-	[29]
$SmBaCo_2O_{5+\delta}$	749	627	-	-	-	21.1	[62]
$SmBaCo_2O_{5+\delta}$	-	-	-	1.60	-	-	[40]
$SmBaCo_2O_{5+\delta}$	-	-	0.52	0.10	1.23	-	[63]
$SmSrCo_2O_{5+\delta}$	2137	1585	0.28	-	-	-	[61]
$SmSrCo_2O_{5+\delta}$	615	502	-	0.07	-	22.7	[64]
$SmSrCoMnO_{5+\delta}$	39.5	45.9	-	-	-	13.8	[64]
$SmBa_{0.5}Sr_{0.5}Co_2O_{5+\delta}$	-	-	0.74	0.35	-	-	[65]
$SmBa_{0.5}Sr_{0.5}Co_2O_{5+\delta}$	-	-	0.81	0.35	1.07	-	[47]
$SmBaCo_{1.4}Fe_{0.6}O_{5+\delta}$	275	230	-	-	-	21.2	[62]
$SmBaCo_{1.6}Fe_{0.4}O_{5+\delta}$	342	283	-	-	-	20.8	[62]
$SmBaCo_{1.6}Ni_{0.4}O_{5+\delta}$	413	329	-	-	-	20.6	[50]
$SmBaCo_{1.8}Fe_{0.2}O_{5+\delta}$	483	395	-	-	-	20.4	[62]
$SmSrCo_{1.2}Mn_{0.8}O_{5+\delta}$	70.5	76.0	-	0.14	1.29	17.4	[64]
$SmSrCo_{1.4}Mn_{0.6}O_{5+\delta}$	118	110	-	0.11	1.02	18.1	[64]
$SmSrCo_{1.6}Mn_{0.4}O_{5+\delta}$	203	173	-	0.09	1.28	20.7	[64]
$SmSrCo_{1.8}Mn_{0.2}O_{5+\delta}$	358	296	-	0.08	1.19	21.3	[64]
$SmBa_{0.5}Sr_{0.5}Co_{1.5}Fe_{0.5}O_{5+\delta}$	261	245	32.2	6.31	-	-	[66]

$Sm_{0.92}BaCo_2O_{5+\delta}$	576	472	-	-	-	-	**[63]**
$Sm_{0.95}BaCo_2O_{5+\delta}$	503	411	0.32	0.07	1.06	-	**[63]**
$Sm_{0.97}BaCo_2O_{5+\delta}$	371	302	0.32	0.07	1.07	-	**[63]**
$SmBa_{0.25}Sr_{0.75}Co_2O_{5+\delta}$	1373	1049	0.14	-	-	-	**[61]**
$SmBa_{0.50}Sr_{0.50}Co_2O_{5+\delta}$	1006	787	0.14	-	-	-	**[61]**
$SmBa_{0.75}Sr_{0.25}Co_2O_{5+\delta}$	741	577	0.17	-	-	-	**[61]**

Table 8. Composition, synthetic route, sintering temperature, lattice type and parameters and oxygen content of Sm-based double perovskite cathodes.

COMPOSITION	**Synthesis Method**	**Sintering Temp [°C]**	**Lattice type**	***a* [Å]**	***b* [Å]**	***c* [Å]**	**Oxygen content [5+δ]**	**Reference**
$SmBaCo_2O_{5+\delta}$	SS	1100	O	3.886	7.833	7.560	5.60	**[53]**
$SmBaCo_2O_{5+\delta}$	SS	1100	T	3.928	-	7.540	5.69	**[33]**
$SmBaCo_2O_{5+\delta}$	SS	1100	O	3.880	3.907	7.559	5.65	**[20]**
$SmBaCo_2O_{5+\delta}$	P	1100	O	3.900	3.918	7.591	5.62	**[61]**
$SmBaCo_2O_{5+\delta}$	SS	1100	O	3.886	7.833	7.560	5.61	**[54]**
$SmBaCo_2O_{5+\delta}$	SS	1100	T*	3.886	3.909	7.566	5.40	**[19]**
$SmBaCo_2O_{5+\delta}$	SS	1100	-	-	-	-	5.54	**[18]**
$SmBaCo_2O_{5+\delta}$	SG	1150	O	3.866	3.885	7.569	5.68	**[29]**
$SmBaCo_2O_{5+\delta}$	C	1100	O	3.889	7.839	7.563	5.61	**[62]**
$SmBaCo_2O_{5+\delta}$	SG	1150	O	3.898	3.887	7.561	5.46	**[63]**
$SmSrCo_2O_{5+\delta}$	P	1150	O	5.403	5.383	7.626	6.00	**[61]**
$SmBaCo_{1.4}Fe_{0.6}O_{5+\delta}$	C	1100	T	3.904	-	7.618	5.76	**[62]**
$SmBaCo_{1.6}Fe_{0.4}O_{5+\delta}$	C	1100	O	3.888	7.826	7.599	5.74	**[62]**
$SmBaCo_{1.6}Ni_{0.4}O_{5+\delta}$	SG	1200	O	3.916	3.887	7.577	-	**[50]**
$SmBaCo_{1.8}Fe_{0.2}O_{5+\delta}$	C	1100	O	3.888	7.828	7.579	5.71	**[62]**
$SmBa_{0.5}Sr_{0.5}Co_{1.5}Fe_{0.5}O_{5+\delta}$	SG	1200	T	3.865	-	7.610	-	**[66]**
$Sm_{0.95}BaCo_2O_{5+\delta}$	SG	1150	O	3.902	3.889	7.569	5.37	**[63]**

$Sm_{0.97}BaCo_2O_{5+\delta}$	SG	1150	O	3.902	3.888	7.567	5.36	**[63]**
$SmBa_{0.25}Sr_{0.75}Co_2O_{5+\delta}$	P	1150	T	3.834	-	7.664	5.87	**[61]**
$SmBa_{0.50}Sr_{0.50}Co_2O_{5+\delta}$	P	1150	T	3.867	-	7.586	5.76	**[61]**
$SmBa_{0.75}Sr_{0.25}Co_2O_{5+\delta}$	P	1150	O	3.886	3.891	7.589	5.70	**[61]**

* tetragonal with orthorhombic superstructure

Conductivity differences in the reported $SmBaCo_2O_{5+\delta}$ compounds are quite high (see Table7, Ref.[20] and [29]). Largely, high conductivity values (> 100 $S \cdot cm^{-1}$) are reported except for Mn bearing compounds where it is significantly lower (Table 7, Ref. [64]. The lowest reported ASR values are 0.10 $\Omega \cdot cm^2$ at 700 °C for $SmBaCo_2O_{5+\delta}$ (Table 7, Ref.[63] and 0.07 $\Omega \cdot cm^2$ in $SmSrCo_2O_{5+\delta}$ (Ref. [64]). Oxygen contents of 5.40÷5.69 are reported for undoped $SmBaCo_2O_{5+\delta}$ while it extends to 5.36÷6.00 taking into account the doped compounds. Despite the poor conductivities obtained, the samples doped with manganese allow lowering the TEC values, down to about 13.8 [10^6 K^{-1}] (Table 7, Ref. [64]).

Table 9 reports some selected electrochemical and thermal parameters of Gd-based compounds; table 10 reports other relevant chemical and physical parameters and the preparation method and temperature for the same compounds.

Table 9. Composition, electrical conductivity σ, ASR and TEC of Gd-based double perovskite cathodes

COMPOSITION	σ @ 600 °C [S·cm^{-1}]	σ @ 700 °C [S·cm^{-1}]	ASR @ 600 °C [Ω·cm^2]	ASR @ 700 °C [Ω·cm^2]	E att [eV]	TEC [10^6 K^{-1}]	Reference
$GdBaCo_2O_{5+\delta}$	483	377	-	-	-	16.6	**[67]**
$GdBaCo_2O_{5+\delta}$	-	-	-	-	-	20.1	**[53]**
$GdBaCo_2O_{5+\delta}$	-	-	1.73	-	1.34	-	**[68]**
$GdBaCo_2O_{5+\delta}$	-	-	3.10	-	-	-	**[68]**
$GdBaCo_2O_{5+\delta}$	-	-	1.35	-	1.27	-	**[68]**
$GdBaCo_2O_{5+\delta}$	375	359	2.11	0.34	1.21	18.1	**[36]**
$GdBaCo_2O_{5+\delta}$	-	-	1.08	0.12	1.43	-	**[69]**
$GdBaCo_2O_{5+\delta}$	512	406	-	-	-	16.6	**[20]**
$GdBaCo_2O_{5+\delta}$	-	-	-	-	-	-	**[27]**
$GdBaCo_2O_{5+\delta}$	231	198	0.42	0.04	-	-	**[27]**
$GdBaCo_2O_{5+\delta}$	210	179	0.18	0.01	-	-	**[27]**
$GdBaCo_2O_{5+\delta}$	-	-	-	-	-	18.4	**[70]**
$GdBaCo_2O_{5+\delta}$	-	-	-	-	-	18.4	**[70]**
$GdBaCo_2O_{5+\delta}$	-	-	21.7	5.77	-	-	**[26]**
$GdBaCo_2O_{5+\delta}$	105	89.9	0.25	0.03	-	-	**[29]**
$GdBaCo_2O_{5+\delta}$	-	-	2.44	0.40	-	-	**[40]**
$GdBaCo_2O_{5+\delta}$	-	-	0.40	0.08	-	20.8	**[71]**
$GdBaCo_2O_{5+\delta}$	-	-	1.14	0.43	-	19.9	**[72]**
$GdBaCo_2O_{5+\delta}$	484	378	2.54	0.87	1.75	19.9	**[56]**
$GdBaCoCuO_{5+\delta}$	50.8	68.3	4.78	0.65	-	-	**[57]**
$GdBaCoCuO_{5+\delta}$	-	-	2.48	0.68	-	13.9	**[72]**
$GdBaCoFeO_{5+\delta}$	73.6	70.9	3.38	1.09	1.86	18.8	**[56]**
$GdSrCo_2O_{5+\delta}$	1155	934	-	-	1.29	18.8	**[67]**

$GdBa_{0.4}Sr_{0.6}Co_2O_{5+\delta}$	1111	932	-	-	-	19.5	**[67]**
$GdBa_{0.5}Sr_{0.5}Co_2O_{5+\delta}$	-	-	1.11	0.55	1.22	-	**[47]**
$GdBa_{0.5}Sr_{0.5}Co_2O_{5+\delta}$	2178	2031	-	-	-	-	**[73]**
$GdBa_{0.5}Sr_{0.5}Co_2O_{5+\delta}$	640	521	0.13	-	-	-	**[74]**
$GdBa_{0.5}Sr_{0.5}CoCuO_{5+\delta}$	64.1	66.2	7.21	0.84	-	-	**[57]**
$GdBa_{0.5}Sr_{0.5}CoFeO_{5+\delta}$	66.6	56.9	-	-	-	-	**[73]**
$GdBa_{0.5}Sr_{0.5}CoFeO_{5+\delta}$	27.5	25.0	0.08	-	-	-	**[74]**
$GdBa_{0.6}Sr_{0.4}Co_2O_{5+\delta}$	1023	821	-	-	-	18.3	**[67]**
$GdBa_{0.8}Sr_{0.2}Co_2O_{5+\delta}$	804	664	-	-	-	18.0	**[67]**
$GdBaCo_{1.5}Fe_{0.5}O_{5+\delta}$	274	229	1.21	0.56	1.20	19.6	**[56]**
$GdBaCo_{1.7}Ni_{0.3}O_{5+\delta}$	-	-	0.55	0.15	-	15.5	**[71]**
$GdBaCo_{1.8}Ni_{0.2}O_{5+\delta}$	-	-	0.48	0.14	-	17.1	**[71]**
$GdBaCo_{1.9}Ni_{0.1}O_{5+\delta}$	-	-	0.44	0.12	-	18.9	**[71]**
$GdBaCuCo_{0.5}Fe_{0.5}O_{5+\delta}$	7.5	9.9	-	1.40	-	14.4	**[75]**
$GdBa_{0.5}Sr_{0.5}Co_{0.5}Fe_{1.5}O_{5+\delta}$	8.3	8.8	-	-	-	-	**[73]**
$GdBa_{0.5}Sr_{0.5}Co_{1.5}Fe_{0.5}O_{5+\delta}$	694	620	2.33	0.96	-	21.8	**[73]**
$GdBa_{0.5}Sr_{0.5}Co_{1.5}Fe_{0.5}O_{5+\delta}$	261	225	0.10	-	-	-	**[74]**
$GdBa_{0.25}Sr_{0.75}CoCuO_{5+\delta}$	30.7	37.3	6.11	0.80	1.05	-	**[57]**
$GdBa_{0.75}Sr_{0.25}CoCuO_{5+\delta}$	39.5	47.6	6.11	0.80	-	-	**[57]**
$GdBaCo_{0.66}Fe_{0.66}Cu_{0.66}O_{5+\delta}$	-	-	1.56	0.46	-	14.6	**[72]**
$GdBaCo_{0.66}Fe_{0.66}Ni_{0.66}O_{5+\delta}$	-	-	1.91	0.54	-	17.5	**[72]**

Table 10. Composition, synthetic route, sintering temperature, lattice type and parameters and oxygen content of Gd-based double perovskite cathodes.

COMPOSITION	**Synthesis Method**	**Sintering Temp [°C]**	**Lattice type**	***a* [Å]**	***b* [Å]**	***c* [Å]**	**Oxygen content [5+δ]**	**Reference**

$GdBaCo_2O_{5+\delta}$	SS	1000	O	3.876	3.912	7.541	5.61	**[67]**
$GdBaCo_2O_{5+\delta}$	SS	1100	O	3.875	7.822	7.533	5.53	**[53]**
$GdBaCo_2O_{5+\delta}$	SS	1000	O	-	-	-	5.48	**[36]**
$GdBaCo_2O_{5+\delta}$	SS	1100	O	3.873	3.912	7.529	5.57	**[20]**
$GdBaCo_2O_{5+\delta}$	SS	1200	T	-	-	-	5.30	**[27]**
$GdBaCo_2O_{5+\delta}$	SS	1200	O	-	-	-	5.80	**[27]**
$GdBaCo_2O_{5+\delta}$	SS	1200	T	-	-	-	5.40	**[27]**
$GdBaCo_2O_{5+\delta}$	SS	1100	T*	3.875	3.911	7.534	5.40	**[19]**
$GdBaCo_2O_{5+\delta}$	SS	1100	-	-	-	-	5.42	**[18]**
$GdBaCo_2O_{5+\delta}$	SG	1150	O	3.860	3.861	7.519	5.66	**[29]**
$GdBaCo_2O_{5+\delta}$	SS	1100	O	3.877	7.825	7.542	5.57	**[56]**
$GdBaCoCuO_{5+\delta}$	SS	1000	T	3.894	-	7.604	5.64	**[57]**
$GdBaCoFeO_{5+\delta}$	SS	1100	T	3.903	-	7.643	6.00	**[56]**
$GdSrCo_2O_{5+\delta}$	SS	1000	O	5.373	5.402	7.572	6.00	**[67]**
$GdBa_{0.4}Sr_{0.6}Co_2O_{5+\delta}$	SS	1000	T	3.840	-	7.549	5.83	**[67]**
$GdBa_{0.5}Sr_{0.5}Co_2O_{5+\delta}$	P	1100	T	3.862	-	7.558	-	**[74]**
$GdBa_{0.5}Sr_{0.5}CoCuO_{5+\delta}$	SS	1000	T	3.866	-	7.576	5.66	**[57]**
$GdBa_{0.5}Sr_{0.5}CoFeO_{5+\delta}$	P	1150	T	3.871	-	7.637	-	**[74]**
$GdBa_{0.6}Sr_{0.4}Co_2O_{5+\delta}$	SS	1000	T	3.856	-	7.546	5.79	**[67]**
$GdBa_{0.8}Sr_{0.2}Co_2O_{5+\delta}$	SS	1000	T	3.872	-	7.550	5.69	**[67]**
$GdBaCo_{1.5}Fe_{0.5}O_{5+\delta}$	SS	1100	T	3.895	-	7.592	5.98	**[56]**
$GdBa_{0.5}Sr_{0.5}Co_{1.5}Fe_{0.5}O_{5+\delta}$	P	1150	T	3.869	-	7.594	-	**[74]**
$GdBa_{0.25}Sr_{0.75}CoCuO_{5+\delta}$	SS	1000	T	3.880	-	7.593	5.58	**[57]**
$GdBa_{0.75}Sr_{0.25}CoCuO_{5+\delta}$	SS	1000	T	3.880	-	7.596	5.68	**[57]**
$GdBaCo_{0.66}Fe_{0.66}Cu_{0.66}O_{5+\delta}$	SG	1000	T	3.885	-	7.635	-	**[72]**

* tetragonal with orthorhombic superstructure

Gd-based compounds seem to grant very low ASR values in some compositions (Table 9, Ref. [27], [29] and [71]) while the reported conductivities reach the highest values only in Sr-doped compounds (Table 7, Ref. [67], [73]) while the double doping with Sr- and Fe- depresses the conductivity again (Table 7 Ref. [74] and [73]). The reported TEC values are in many references

considerably lower respect to the values of analogous Pr-, Nd- and Sm- based samples. Except for the very high values reported in Ref.[56] and [67] (i.e. 6.00 and 5.98) the oxygen content range is 5.40÷5.83 mole of oxygen per mole of compound.

Table 11 reports some selected electrochemical and thermal parameters of Y-based compounds; table 12 reports other relevant chemical and physical parameters and the preparation method and temperature for the same compounds.

Table 11. Composition, electrical conductivity σ, ASR and TEC of Y-based double perovskite cathodes

COMPOSITION	**σ @ 600 °C [S·cm^{-1}]**	**σ @ 700 °C [S·cm^{-1}]**	**ASR @ 600 °C [Ω·cm^2]**	**ASR @ 700 °C [Ω·cm^2]**	**E att [eV]**	**TEC [10^6 K^{-1}]**	**Reference**
$YBaCo_2O_{5+\delta}$	189	160	-	-	-	16.3	**[25]**
$YBaCo_2O_{5+\delta}$	189	160	-	0.11	0.49	16.3	**[25]**
$YBaCo_2O_{5+\delta}$	23.6	21.2	0.53	0.13	0.92	-	**[30]**
$YBaCo_2O_{5+\delta}$	135	121	3.93	1.03	-	-	**[66]**
$YBaCo_2O_{5+\delta}$	-	-	-	-	-	13.8	**[53]**
$YBaCo_2O_{5+\delta}$	69.8	58.5	-	0.09	-	17.8	**[24]**
$YBaCo_2O_{5+\delta}$	119	120	0.99	0.21	-	-	**[76]**
$YBaCo_2O_{5+\delta}$	215	178	-	-	-	-	**[77]**
$YBaCo_2O_{5+\delta}$	153	122	-	-	-	15.8	**[20]**
$YBaCo_2O_{5+\delta}$	-	-	-	-	-	19.1	**[23]**
$YBaCo_2O_{5+\delta}$	24.9	-	-	-	-	-	**[78]**
$YBaCo_2O_{5+\delta}$	37.8	31.7	4.59	0.63	-	-	**[29]**
$YSrCo_2O_{5+\delta}$	-	-	1.37	0.41	0.97	-	**[23]**
$YBa_{0.2}Sr_{0.8}Co_2O_{5+\delta}$	-	-	1.34	0.22	1.50	-	**[23]**
$YBa_{0.3}Sr_{0.7}Co_2O_{5+\delta}$	-	-	1.08	0.17	1.50	-	**[23]**

$YBa_{0.4}Sr_{0.6}Co_2O_{5+\delta}$	-	-	1.55	0.24	1.50	19.8	**[23]**
$YBa_{0.5}Sr_{0.5}Co_2O_{5+\delta}$	424	337	-	-	-	18.8	**[25]**
$YBa_{0.5}Sr_{0.5}Co_2O_{5+\delta}$	371	291	1.78	0.36	1.21	-	**[76]**
$YBa_{0.5}Sr_{0.5}Co_2O_{5+\delta}$	70.3	59.4	-	-	-	-	**[78]**
$YBa_{0.6}Sr_{0.4}Co_2O_{5+\delta}$	318	283	2.24	0.35	-	-	**[76]**
$YBa_{0.7}Sr_{0.3}Co_2O_{5+\delta}$	512	450	3.29	0.57	-	-	**[76]**
$YBa_{0.8}Sr_{0.2}Co_2O_{5+\delta}$	445	396	1.07	0.20	-	-	**[76]**
$YBa_{0.9}Sr_{0.1}Co_2O_{5+\delta}$	165	145	2.04	0.46	-	-	**[76]**
$YBaCo_{1.2}Cu_{0.8}O_{5+\delta}$	27.9	38.3	-	0.18	-	13.4	**[24]**
$YBaCo_{1.2}Fe_{0.8}O_{5+\delta}$	23.3	20.7	-	-	-	-	**[77]**
$YBaCo_{1.4}Cu_{0.6}O_{5+\delta}$	39.8	47.4	-	0.12	-	14.7	**[24]**
$YBaCo_{1.4}Fe_{0.6}O_{5+\delta}$	27.1	22.6	-	-	-	-	**[25]**
$YBaCo_{1.4}Fe_{0.6}O_{5+\delta}$	44.1	36.4	-	-	-	-	**[77]**
$YBaCo_{1.6}Cu_{0.4}O_{5+\delta}$	55.4	57.8	-	0.18	-	15.7	**[24]**
$YBaCo_{1.6}Fe_{0.4}O_{5+\delta}$	55.9	47.1	-	0.15	0.53	18.0	**[25]**
$YBaCo_{1.6}Fe_{0.4}O_{5+\delta}$	64.7	53.4	-	-	-	-	**[77]**
$YBaCo_{1.8}Cu_{0.2}O_{5+\delta}$	67.1	71.6	-	0.15	-	16.7	**[24]**
$YBaCo_{1.8}Fe_{0.2}O_{5+\delta}$	128	107	-	0.13	0.52	17.3	**[25]**
$YBaCo_{1.8}Fe_{0.2}O_{5+\delta}$	136	112	-	-	-	-	**[77]**
$YBa_{0.5}Sr_{0.5}Co_{1.4}Cu_{0.6}O_{5+\delta}$	114	106	-	0.18	1.18	16.4	**[79]**

Table 12. Composition, synthetic route, sintering temperature, lattice type and parameters and oxygen content of Y-based double perovskite cathodes.

COMPOSITION	**Synthesis Method**	**Sintering Temp [°C]**	**Lattice type**	***a* [Å]**	***b* [Å]**	***c* [Å]**	**Oxygen content [5+δ]**	**Reference**
$YBaCo_2O_{5+\delta}$	SS	1100	T	3.879	-	7.509	-	**[25]**
$YBaCo_2O_{5+\delta}$	SG	1050	T	3.874	-	7.502	-	**[66]**
$YBaCo_2O_{5+\delta}$	SS	1100	T	11.616	-	7.493	5.51	**[53]**

$YBaCo_2O_{5+\delta}$	SG	1000	T	11.627	-	7.509	-	**[24]**
$YBaCo_2O_{5+\delta}$	SS	1100	T	11.615	-	7.496	-	**[77]**
$YBaCo_2O_{5+\delta}$	SS	1100	T	3.874	-	7.483	5.41	**[20]**
$YBaCo_2O_{5+\delta}$	SS	1125	T	3.878	-	7.498	5.31	**[23]**
$YBaCo_2O_{5+\delta}$	SG	1150	O	3.846	3.954	7.485	5.41	**[29]**
$YBa_{0.3}Sr_{0.7}Co_2O_{5+\delta}$	SS	1125	T	-	-	-	5.54	**[23]**
$YBa_{0.4}Sr_{0.6}Co_2O_{5+\delta}$	SS	1125	T	-	-	-	5.50	**[23]**
$YBa_{0.5}Sr_{0.5}Co_2O_{5+\delta}$	SS	1125	-	-	-	-	5.40	**[23]**
$YBaCo_{1.2}Cu_{0.8}O_{5+\delta}$	SG	1000	T	11.658	-	7.551	-	**[24]**
$YBaCo_{1.2}Fe_{0.8}O_{5+\delta}$	SS	1100	T	11.632	-	7.566	-	**[77]**
$YBaCo_{1.4}Cu_{0.6}O_{5+\delta}$	SG	1000	T	11.658	-	7.546	-	**[24]**
$YBaCo_{1.4}Fe_{0.6}O_{5+\delta}$	SS	1100	T	3.893	-	7.555	-	**[25]**
$YBaCo_{1.4}Fe_{0.6}O_{5+\delta}$	SS	1100	T	11.637	-	7.554	-	**[77]**
$YBaCo_{1.6}Cu_{0.4}O_{5+\delta}$	SG	1000	T	11.656	-	7.541	-	**[24]**
$YBaCo_{1.6}Fe_{0.4}O_{5+\delta}$	SS	1100	T	3.885	-	7.535	-	**[25]**
$YBaCo_{1.6}Fe_{0.4}O_{5+\delta}$	SS	1100	T	11.636	-	7.532	-	**[77]**
$YBaCo_{1.8}Cu_{0.2}O_{5+\delta}$	SG	1000	T	11.648	-	7.534	-	**[24]**
$YBaCo_{1.8}Fe_{0.2}O_{5+\delta}$	SS	1100	T	3.881	-	7.519	-	**[25]**
$YBaCo_{1.8}Fe_{0.2}O_{5+\delta}$	SS	1100	T	11.623	-	7.529	-	**[77]**

As already mentioned, undoped $YBaCo_2O_{5+\delta}$ is prone to decomposition by simple heat treatment at high temperature in air, but its structure can be stabilized by proper doping [24]; Focusing then on doped compounds, it is worth noting that the electrical conductivity values are much lower than the Pr- and Nd-based counterparts, with a few composition cross the threshold of 100 $S \cdot cm^{-1}$ (Table 11, Ref. [25], [76], and in a minor extent Ref. [77] and [79]). Except for the results Zhang et al. (Table 12, Ref. [29]) all the reported Y bearing compounds adopt a tetragonal lattice. A few measurements are available of the oxygen content, that is indeed significantly lower than in the other examined rare earth double perovskites (= 5.31÷5.51).

For sake of completeness, Table 13 reports the relevant chemical and physical parameters: preparation method, sintering temperature, lattice type and cell parameters, oxygen content for other minor rare earths based compounds, for which electrochemical measurements are not reported.

Tabe 13. Composition, synthetic route, sintering temperature, lattice type and parameters and oxygen content of Dy, Eu, Ho and Tb based double perovskite cathodes.

COMPOSITION	**Synthesis Method**	**Sintering Temp [°C]**	**Lattice type**	***a* [Å]**	***b* [Å]**	***c* [Å]**	**Oxygen content [5+δ]**	**Reference**
$DyBaCo_2O_{5+\delta}$	SS	1100	T	3.879	-	7.505	-	**[53]**
$DyBaCo_2O_{5+\delta}$	SS	1100	T	3.876	3.879	7.504	5.30	**[19]**
$DyBaCo_2O_{5+\delta}$	SS	1100	-	-	-	-	5.36	**[18]**
$EuBaCo_2O_{5+\delta}$	SS	1100	O	3.882	7.828	7.546	5.56	**[53]**
$EuBaCo_2O_{5+\delta}$	SS	1100	T	3.883	3.916	7.541	5.40	**[19]**
$EuBaCo_2O_{5+\delta}$	SS	1100	-	-	-	-	5.52	**[18]**
$HoBaCo_2O_{5+\delta}$	SS	1100	T	3.873	-	7.495	-	**[53]**
$HoBaCo_2O_{5+\delta}$	SS	1125	T	3.882	-	7.488	5.14	**[23]**
$HoBaCo_2O_{5+\delta}$	SS	1100	T	3.873	3.872	7.496	5.30	**[19]**
$HoBaCo_2O_{5+\delta}$	SS	1100	-	-	-	-	5.25	**[18]**
$TbBaCo_2O_{5+\delta}$	SS	1100	O	3.868	7.818	7.518	-	**[53]**
$TbBaCo_2O_{5+\delta}$	SS	1100	T	3.867	3.908	7.516	5.40	**[19]**
$TbBaCo_2O_{5+\delta}$	SS	1100	-	-	-	-	5.41	**[18]**

As mentioned above, A site cation dimension is known to have an influence on crystal structure and on the electrochemical properties: at a first sight, it can be stated that the best performance are obtained when middle-sized ions occupy the A site (praseodymium, neodymium, samarium and gadolinium); in Table 14 the ionic size of the investigated A site cations are reported as the effective ionic radius of the 12-fold coordinated ion when available, or as the size of the 9-fold coordinated ion [80], [81]. In the end, it appears that these elements provide a good trade-off between electrochemical activity and TEC. This is not surprising, as it has been shown that both TEC and electrical conductivity generally decrease reducing the size of the rare earth ion in *RE*$BaCo_2O_{5+\delta}$ [20]. Thus, a detailed analysis has been performed on the compounds with the mentioned elements on the A site. However, also Y-based compounds look quite promising in some compositions, because they keep the lowest TEC values in the series, which better mimic the thermal expansion coefficients of the common intermediate temperature electrolytes. Therefore also Y-based compounds will be occasionally mentioned, in some specific compositions, to illustrate the general trends in the investigated properties and the effects of doping on the electrochemical performance.

Table 14: effective ionic radii rare earths (12-fold coordination, from [80]; * 9-fold coordination, from [81])

Rare Earth Ion	**Effective Ionic Radius**
Y^{3+}	1.075*
La^{3+}	1.36
Pr^{3+}	1.32
Nd^{3+}	1.31

Sm^{3+}	1.28
Gd^{3+}	1.27
Eu^{3+}	1.28
Dy^{3+}	1.24
Ho^{3+}	1.23
Tb^{3+}	1.25

The analysis of the results reported in the available literature faces a complication that somehow hinders the understanding of the key factors affecting the effectiveness of cathodic materials. This issue is the high spread of results, especially in term of conductivity and ASR results reported for homologous compounds. From Tables 1-3-5-7-9-11, it is noticeable that the same compound, synthesized by different researchers or under slight different conditions, often shows very dissimilar values of the relevant electrochemical parameters.

To put this fact in better evidence, Figure 1 shows a general overview of all the electric conductivity values reported for the investigated compounds. They are grouped by the A site rare earth: Pr, Nd, Gd, Sm and Y respectively. For each A site element, conductivity values are reported for every composition, split in quartiles: 50% of the intermediate values are shown with the bar, while the lowest 25% of the values is represented by the line in the bottom part and the highest 25% with line on top of the bars, at each reported temperature, from 500 to 850 °C at 50 °C interval. This representation allows to visualize the spread of conductivity values for each *RE* based perovskite, and underlines the huge difference in conductivity that can be obtained by varying the substitution and stoichiometry of the compounds. The number of Pr-based compounds in the retrieved papers are more than 40, while others rare earth perovskites reach a number of compounds between 22 (for Sm) and 30 (for Y). In addition, it’s easy to visualize that yttrium based perovskites present

conductivity values in average lower than 100 $S \cdot cm^{-1}$. This conductivity is actually considered a threshold value for a successful application as cathode materials according to Steele [82].

A similar graph is reported in Figure 1B for the ASR values. For this parameter, the number of available measurements is not the same at each temperature shown; actually most authors report ASR values measured in the temperature range 600÷800 °C, and some only report a few values measured at 700 or 750 °C. That temperature range shall therefore be considered the more reliable one. Considering Pr-based perovskites, retrieved ASR values for 650-700 °C temperature range are about 35, while for other temperatures even less than 20. Other A site compounds present similar trend with number of data between 20 and 30 for 650-700 °C range and about half measurements available at the other temperatures. An indicative values range of ASR in order to consider a material suitable for cathodic application is between 0.10 and 0.20 $\Omega \cdot cm^2$ reported by Steele at al. [82]. It must be noted that only few compositions fulfill this condition in the intermediate temperature range (600 °C). The number of compounds that satisfy this requirement of course increases at higher temperatures (700-750 °C), especially in Pr-based compounds.

The wide spread of results is related to many factors, involving both the processes of synthesis and measurement. First of all, comparing different materials with same A site element can lead to a considerable number of possible compositions with several chemical and structural modifications that strongly influence the measured parameters. These differences in conductivity and ASR results for homologous compounds may be explained by the issue of synthesizing materials with a sharp accuracy in the final composition. Unfortunately, slight variations of few percent in the compositions can lead to significant changes in the electric and electrochemical performance, as shown in some recent papers dealing with cationic deficiency in double perovskites. In fact, a slight change in composition and/or lattice parameters strongly affects the properties of the solid compound [63, 83-88]. Therefore, in absence of an accurate stoichiometry determination, the comparison between nominally equal compounds could lead to misinterpretation of the results. In

addition, the high sensitivity of the electrochemical properties to slight variations in the cation and anion stoichiometry increases the need of accurate synthetic procedures.

An even higher irregularity was observed when analyzing ASR values retrieved in literature: a deviation of up to two orders of magnitude can be found in similar materials. This can be explained by the numerous chemical, physical and microstructural parameters actually affecting the results of impedance spectroscopy measurements.

3.2. Electrochemical Performance

An optimization of the composition of double perovskites is required in order to reach the best tradeoff between electrochemical performance and cell durability. The electrochemical performance of IT-SOFC cathodes is commonly assessed by measurement of two electrochemical parameters: ASR and electrical conductivity. The first one represents the global resistance opposed by the material layer to all the chemical, diffusive and electrical processes occurring at the cathode, and it should be minimized. The conductivity, instead, is the measure of the attitude to conduct electric charge, and needs to be as high as possible.

The ASR value includes material data about the electrons and ions transfer processes occurring at the current collector-electrode-electrolyte interfaces, and about non-charge transfer processes including oxygen surface exchange, solid-state diffusion, and gas-phase diffusion inside and outside the electrode [89]. Therefore both chemical and microstructural parameters can affect ASR.

In order to measure the ASR value, cathodic materials need to be deposited on a pellet made by typical electrolyte materials for IT-SOFC. Thus, the choice of the electrolyte material, the pellet, the layer thickness and adhesion impact on the overall resistance measured. All these elements make the choice of electrolyte used for electrochemical analysis important and not trivial. Has been demonstrated that also the choice of the electrolyte material influences the impedance spectroscopy measurements of the same cathode. This result has been explained by some authors in terms of different contact of the

cathode layer to the electrolyte support [46]. In addition, even the preparation of the cell assembly influences the final ASR value. In fact, same powders can be deposited using different techniques, with different grains sizes, porosity and layer adhesion; the sintering can be performed at different temperatures and for different times, resulting in changes in diffusion paths, number of active sites, connectivity between grains and other elements [5]. The ASR is always monotonically decreasing with increasing the temperature in solid oxides, due to the effect of reduction kinetics and diffusion limitations. The slope of ASR is related to the activation energy of the whole process that brings from O_2 in the gas phase to O^{2-} in the electrolyte, despite the number of possible intermediate steps, and follows an Arrhenius law.

Only a detailed kinetic analysis of the different contributes to the total resistance allows quantifying the real cathode activity effectiveness of the materials; nonetheless, this kind of analysis is often time-consuming, and sometimes it is not easy to isolate the different contribution in the impedance spectra. Of great interest would be a comparison between a complete evaluation and discussion of spectroscopy contributions, in order to figure out how much electrical resistance is produced by macroscopic properties and how much is the actual material contribute. However, since only few papers [24, 30, 58, 65, 79, 86, 90-93] present this accurate analysis, it's still not possible to compare the results, either to reach a helpful conclusion. This leads to a harder comparison of several cathodic materials synthesized by different researchers.

However, the conductivity helps to evaluate the electric efficiency of the materials, measuring the global ability to conduct an electric current. This parameter is composed of two contributes: electronic and ionic conductivities. In order to make a cathodic material satisfying, both conductivities have to be as high as possible. In almost every paper classified, only the global value of conductivity is reported, without subdivision in its two contributes. However, ionic conductivity in these materials is at least two orders of magnitude lower than electronic conductivity, hence the measured value is usually attributed to electronic charge carriers [94].

Double perovskite materials can present different conduction behaviors, based on the temperature dependency of the global conductivity. If the conductivity increases with temperature, the material owns a semiconductor-like behavior, while metallic-like conductivity decreases with increasing temperature. Frequently, double perovskites exhibit both these conductivity mechanisms; a change in the conductivity is observed as a function of temperature: generally, a transition is reported as the shift from semiconductor (at low temperature) to metallic-like behavior (at high temperature) and it follows that these materials exhibit a maximum in the conductivity values at intermediate temperatures. This transition temperature changes depending on the chemical composition, but it's usually situated between 300 and 600 °C. The change in the slope of the conductivity vs temperature is attributed to the loss of oxygen occurring in the lattice when increasing the temperature, caused by the reduction of Co^{4+} ($Co_{Co}^{\bullet}$) to Co^{3+} (Co_{Co}^{x}); the defect reaction that occurs can be represented using Kröger-Vink notation [95]:

$$2Co_{Co}^{\bullet} + O_O^x \leftrightarrow 2Co_{Co}^x + v_O^{\bullet\bullet} + \frac{1}{2}O_2 \qquad (1)$$

In order to maintain charge neutrality, each oxygen vacancy ($v_O^{\bullet\bullet}$) generated in the lattice during the heating process causes the loss of two p-type carriers, ($Co_{Co}^{\bullet}$), resulting in a conductivity decrease [76].

3.3. Chemical compatibility with electrolytes

The chemical compatibility among the cell components is an important requirement for the choice of IT-SOFC materials; an investigation of reactivity of cathode materials with the common electrolytes is therefore mandatory in order to determine an optimal electrode-electrolyte couple.

The material chosen for this application need to be chemically inert with the cathode in order to avoid reaction at the cathode-electrolyte interface. Even if solid oxide fuel cells operate at lower temperature, the interdiffusion of cations at the interface could promote the formation of new phases either in the fabrication step or during the cell operation, possibly leading to the formation of an insulating layer at the interface that would obstruct the ionic and electronic transport. In the last years, many of the interesting double perovskite materials for cathodic application have been characterized also for their reactivity with the common electrolytes.

The most common approach to investigate chemical compatibility is by heating up a physical mixture of cathode and electrolyte powders at high temperature for several hours, then analyzing the occurrence of new phases or interdiffusion by means of X-Ray Diffraction (XRD). In case that all the diffraction peaks can be indexed based on a physical mixture of the two phases, it is concluded that no reaction between the two materials has occurred. This easy and common procedure demonstrates if the cathode material is compatible with selected electrolyte, but it has to be taken only as a preliminary result. In fact, a negative result should be reported as a clear evidence of incompatibility, but a positive one is limited to the analysis condition. Moreover, sometimes no clear evidence of new phase formation or cation interdiffusion can be assessed based only on XRD measurements. By the way, in the investigated literature the chemical compatibility is usually checked by applying relatively mild calcination processes (in the temperature range of 900÷1100 °C for 6÷12 hours) and sometimes even for very short times and low temperatures, suggesting that higher temperatures or longer times would have shown some evidence of reactivity. It’s obvious that SOFC materials will have to operate for long times, therefore a more severe characterization of the reactivity is suggested for a meaningful understanding of the long-term reactivity. In fact, when long-lasting stability tests are performed, the measured ASR values increase over time due to (at least) some microstructural rearrangements at the cathode-electrolyte interface [96, 97].

Among commercially available electrolyte materials, YSZ has been reported to react with several double perovskites materials, such as the $PrBaCo_{2-x}Fe_xO_{5+\delta}$ series [39] where the authors reported reactivity for temperatures as low as 700 °C for 20 h with the appearance of small peaks belonging to $PrCoO_3$ or $PrFeO_3$ phases, while at 900 °C a larger amount of $BaZrO_3$ develops; in $SmBaCo_{2-x}Fe_xO_{5+\delta}$ series [62], the growth of $BaZrO_3$ is identified after annealing at 900 °C for 24 hours that is not influenced by the amount of iron in the structure. Tarancon et al. [98] proposed a complete characterization for $GdBaCo_2O_{5+\delta}$ double perovskite stability, concluding that it presents high reactivity with YSZ even at low temperature (700 °C). However, YSZ isn't commonly considered as promising electrolyte for intermediate temperature range unless it is used in very thin layers, therefore few data are available about its reactivity with double perovskite compounds. LSGM and doped ceria electrolytes (GDC, SDC) instead, show higher ionic conductivity in the intermediate temperature range and are better suited for low-temperature operation [5]. Zhou et al. [99], published their results about the chemical compatibility of $REBaCo_2O_{5+\delta}$ (*RE* = Pr, Nd, Sm and Gd) compounds with samarium doped ceria (SDC) and LSGM, reporting that neither additional peaks nor structural changes were detected after 5 hours at 1000 °C. Several other works instead, report reaction issues for compatibility tests performed in more harsh conditions, especially for LSGM as electrolyte: Tarancon et al. [98] investigated the stability of $GdBaCo_2O_{5+\delta}$ also with GDC and LSGM and found the formation of a small amount of secondary phase with both electrolyte materials after annealing at 1000 °C. Moreover, the secondary phase content increases at higher temperature, producing at 1200 °C a solid solution between $GdBaCo_2O_{5+\delta}$ and LSGM with a mixed cubic perovskite lattice; this result is ascribed to the similar lattice structures between the two compounds. It's common that the more the lattices are similar between cathode and electrolyte, the easier is the occurrence of interface reaction. In fact, in materials with the same structure, the diffusion of ions across the interface in order to reduce ionic gradient faces low activation energy. Therefore it's expected that double perovskite materials could present more reactivity issues with LSGM, a single doped perovskite ($A_{1-x}A'_xB_{1-y}B'_yO_3$), than with GDC or SDC, doped ceria

electrolytes ($A_{1-x}A'_xO_2$) that adopt a fluorite structure. In fact, among available electrolyte materials, GDC or SDC series result more often used in the recent literature.

The doping effect on chemical stability is different based on material properties: Y-based double perovskites usually present a phase instability when undoped, while has been demonstrated that the substitution of Ba with Sr enhance the not only the chemical stability but also the compatibility with GDC electrolyte [23, 67]. In addition, a proper amount of Sr substitution into the double perovskite composition could reduce the ion diffusion issue with LSGM electrolyte, because it could reduce the sharp concentration gradient of Sr at the cathode-electrolyte interface. However, sometimes the presence of a dopant element can worsen the electrolyte-electrode compatibility, because it could promote the formation of a more thermodynamically stable phase during high temperature treatments. Jin et al. [59] for example reported the formation of a secondary phase, $SmCu_2O_4$, at the interface between SDC and $NdBaCo_{0.66}Fe_{0.66}Cu_{0.66}O_{5+\delta}$ after calcination at 950 °C for 10 h in air. On the contrary, the same compoundwas found to be inert with GDC and LSGM at the same calcination conditions.

3.4. Thermal expansion mismatch

Besides electrochemical performance, another important feature of a cathode material is its influence on cell lifetime. Reactivity with the electrolyte materials has been already discussed, but in order to extend the cell durability it is important to have similar TEC values between the cathode and the electrolyte materials (and also the anode of course). A minimum thermal mismatch is required to reduce the strain at the interface occurring during the thermal cycles of the cell. Co based double perovskites usually present a much higher TEC value than typical electrolytes (10.4 - $12.3 \cdot 10^6$ K^{-1} for LSGM series [100] and 11.4 - $12.7 \cdot 10^6$ K^{-1} for rare earths doped ceria [101]). High TECs are related to Co^{3+} cations state, that, at high temperature, can pass from low spin (LS, $t^6_{2g}e^0_g$) to intermediate (IS, $t^5_{2g}e^1_g$) and to high spin (HS, $t^4_{2g}e^2_g$), progressively increasing ionic radius [102]. Hence, to reduce TEC for these materials, Co is partially or completely substituted with different

metals (especially Fe), that can mitigate these disadvantages, trying to maintain good electrochemical performance. In addition, typical dopants cost is often much lower than that of cobalt, reducing the global development cost of a Co based cathodic material [25, 34, 51, 56, 64, 102-104].

In the recent years, another strategy to reduce effectively problems related to TECs mismatch is the use of composite cathodes, that can minimize the undesired thermal expansion discontinuity at the electrolyte-cathode interface, without substituting Co with dopants [90]. A detailed discussion of composite cathode literature is out of the scope of this review, but a brief introduction is reported in the next section.

3.5. Composite cathodes

Initially SOFC developers have used composite materials to improve the performance of the anode [105], then first composite cathodes were studied with the aim of enhancing electrochemical properties for simple perovskite materials. In fact, mixtures with different percentage of electrolytic and cathodic materials were produced and characterized, revealing better performance, most likely caused by the increase of the triple phase boundary length [106, 107]. This effect has been studied even with mathematical models [108-112], resulting in a complex approach, since many side parameters strongly influence the cathode performance. Subsequently, researchers mainly focused their attention on materials that show both ionic and electronic conduction behavior (MIEC), in order to optimize the tradeoff between electronic conductivity and oxygen reduction kinetics [105].

Nowadays, high performance materials have been proposed, and one of the open issues is the high TEC of many of these materials. Instead of reducing TEC values by doping strategies, a recent proposal is to use composite cathodes made by perovskites and electrolytes [58]. In addition, composite cathodes could represent also a breakthrough for oxygen reduction reaction mechanism. In fact, most characterizations about composite cathodes report a decrease in ASR values when composites with around 50% weight ratio of electrolyte material is mixed with the cathodic one.

[65, 105, 106, 113]. However, the addition of electrolyte to cathode materials leads to a significant drop in electronic conductivity; this is often accounted for the decrease in the continuity of the cathodic phase in the composite [105]. A further advancement int composite cathodes is represented by the so-called 'graded' configuration. Graded cathodes are made by different layers of composite cathodes with increasing percentage of electrolyte, in order to gradually reduce the differences in thermal expansion between cathode and electrolyte. The most important aim is to avoid a sharp gap between TEC values, usually presents at the cathode-electrolyte interface. This should greatly improve the cell to withstand many thermal cycles. In addition, a functionally graded cathode can show an enhancement of electrochemical performance even at first measurement, due to the possibility to optimize different parameters for every composite layer [90, 99].

4. Review of the most promising materials

It's very difficult to compare same or similar compounds through different papers because of various production and measurement methods used. Thus, trying to identify general trends across the whole literature about double perovskites could be futile or even counterproductive. However, many publications confirm the positive outcome that McKinlay et al. [78] proposed in their paper in 2007. This work contains a preliminary characterization of the double perovskites with general formula $YBa_{1-x}Sr_xCo_2O_{5+\delta}$ and of particular interest is the marked improvement for conductivity when Sr replaces half Ba.

Many publications confirm this trend, explaining it as a direct cause of the decrease in oxide-ion vacancy concentration due to an increase of both oxygen content and average Co oxidation state, related to Sr^{2+} smaller dimension than Ba^{2+} [42]. Since the oxygen vacancy concentration decreases, the ionic conductivity should decrease too, but the overall conductivity increases due to the higher electronic contribute. In order to increase electronic conductivity, a material needs a large

concentration of electronic holes, elements controlling the ability of moving electrons inside material lattice. However, producing a material with both high electronic and ionic conductivity is quite challenging because any negative charge, such as A site dopants or deficiency, can be compensated by the formation of oxide-ion vacancies or electronic holes, originated by oxidation of Co^{3+} to Co^{4+} [16]. The distribution of these chemical defects is the main factor determining electrical and electrochemical properties of the cathode materials. However, nowadays is not completely known yet what determine the compensation of negative charges by electronic holes or oxygen vacancies.

According to Kim at al. the higher concentration of smaller Co^{4+} ions than Co^{3+} is also related to a relief of the compressive stress in the O−Co−O bonding, that increase toward the ideal value of 180°, causing a structural change from orthorhombic to tetragonal [67]. The tetragonal structure exhibits faster oxygen transport in the bulk and surface and higher catalytic activity for the oxygen reduction reaction as compared to an orthorhombic structure because it provides a more symmetrical structure [55]. Symmetry in cell lattice structure allows a better overlap between 3d orbitales from the transition metal (Co and its dopants) and 2p orbitales from oxygen ions [29, 83, 88].

Electronic conduction within perovskite-related oxides is believed to occur via electron hopping along Co^{4+}−O^{2-}−Co^{3+} bonds. The exact mechanism is thought to resemble a Zerner double exchange process, which is closely related to both the mobility of the electrical carriers and the path of diffusion [29]. Thus, increasing oxygen vacancies impedes the electron hopping pathway and causes a reduction of electronic conductivity [59].

In addition, the complete substitution of Ba with Sr does not produce the alternate double perovskite structure, due to similar radius between rare earths and smaller Sr^{2+}. In fact, even other publications show that $LnSrCo_2O_{5+\delta}$ oxygen content is usually equal to 6, demonstrating that these materials prefer to allocate in disordered $Ln_{0.5}Sr_{0.5}CoO_3$ layers, instead of ordered alternated $LnCoO_3$ and $SrCoO_3$ layers [55, 67]. When δ increases, oxygen ions fill the Ln-O layer, proving pyramidal CoO_5 structures

become octahedral CoO_6, removing lattice charge ordering and reducing crystallographic unit cell along the *b* direction [114]. These simple non-doped perovskites present a very high electrical conductivity due to more symmetric cell structure, usually cubic one. However, these materials do not provide enough oxygen vacancies, resulting in bad ionic conductors. Although adding dopants can produce vacancies thus ionic conduction behavior, it also causes instability and very high TEC [5].

However, focusing only on considerations about conductivity would induce to the production of not optimized materials for cathodes for IT-SOFCs, because maximizing oxygen content leads to very high electronic conductivity values, but it could decrease the ionic one, depending on the defect chemistry of the compound. Low ionic conductivity reveals lack of oxygen vacancies, in advantage of electronic holes, usually causing a reduction of the oxygen surface exchange rate that in turn causes high polarization resistances (ASR) in cases where the surface exchange process is the rate determining step [86].

The lowest ASR reported in literature has been achieved by Choi at al. [45] for the compound with general formula $PrBa_{0.5}Sr_{0.5}Co_{1.5}Fe_{0.5}O_{5+\delta}$. In this paper is reported a value of 0.056 $\Omega \cdot cm^2$ at 600 °C using GDC as electrolyte for the impedance measurements. This publication makes this material more than promising for cathode applications, but in the same year Jiang at al. [49] presented a paper containing the characterization of the same compound, with less promising ASR value. The only value reported by Jiang is 0.07 $\Omega \cdot cm^2$ at 800 °C, even higher than 600 °C for Choi. This discrepancy can be partially explained by the usage of LSGM as electrolyte support in the production of symmetric cells for impedance measures, but it also reveals the difficulty in comparison between same compounds in two different papers.

After McKinlay et al. [78] and Kim et al. [67] publications, many researches followed their steps, producing double perovskites with general formula $LnBa_{0.5}Sr_{0.5}Co_2O_{5+\delta}$, using different rare earths [46, 47, 52, 65, 76, 104] or trying also with B site dopants (Cu [57, 79, 102], Mn [58, 64], Ni [51], Fe

[45, 74]) in order to reduce TEC. However the lowest TEC value has been achieved by Wang et al. that tried to optimize the Mn content in double perovskite $SmSrCo_{2-x}Mn_xO_{5+\delta}$. A value equal to $13.7 \cdot 10^6$ K^{-1} is reported for $SmSrCoMnO_{5+\delta}$, but, although this compound would be suitable for matching with commercial electrolyte TECs, the substitution of half Co leads to a dramatic drop in conductivity from 615 $S \cdot cm^{-1}$ for $SmSrCo_2O_{5+\delta}$ to 40 $S \cdot cm^{-1}$ at 600 °C. In this material larger Mn^{3+} ions replace smaller Co^{3+} causing a bending of (Co,Mn)−O−(Co,Mn) bonds, decreasing the angle below 180 ° and consequently resulting in a metal to semiconductor behavior transition [64].

Kim et al. have produced another Mn-doped double perovskite series with the aims of lowering TEC value and optimizing electrochemical performance. TEC value drops from $20.27 \cdot 10^6$ K^{-1} for $NbBa_{0.5}Sr_{0.5}Co_2O_{5+\delta}$ to $14.33 \cdot 10^6$ K^{-1} for $NbBa_{0.5}Sr_{0.5}Co_{1.5}Mn_{0.5}O_{5+\delta}$. Although a significant drop in performance, both conductivity and ASR are still acceptable for IT-SOFC cathode application. At 600 °C the electrical conductivity of $NbBa_{0.5}Sr_{0.5}Co_{1.5}Mn_{0.5}O_{5+\delta}$ is equal to 717.5 $S \cdot cm^{-1}$ and ASR is 0.1557 $\Omega \cdot cm^2$. Both parameters are worse than respective Mn-free compound (2410 $S \cdot cm^{-1}$ and 0.1154 $\Omega \cdot cm^2$), but Mn-doped material meets the general required value of a cathode material with sufficiently high power density (1.20 $W \cdot cm^{-2}$ at 600 °C) [58].

In order to investigate deeply on material performance, compounds have been divided into different categories based on A site rare earth element. In next sections will be presented a summary of electrochemical parameters for the material series more often synthesized by different authors in literature, *RE*$BaCo_2O_{5+\delta}$ and *RE*$Ba_{0.5}Sr_{0.5}Co_2O_{5+\delta}$., with *RE* = Pr, Nd, Sm and Gd.

4.1. Pr-based double perovskites

Pr-based compounds are the most popular double perovskites present in literature for number of characterization. Figure 2A shows the temperature dependence of the conductivity for the most common Pr-based double perovskite: $PrBaCo_2O_{5+\delta}$. It's evident that there's a large mismatch

between different publications, as conductivity values at 300 °C amount to 200 $S \cdot cm^{-1}$ in the compound investigated by Zhang et al. [29] and reach up to 1500 $S \cdot cm^{-1}$ in the one prepared by Jiang et al.[37]; similarly, at 800 °C σ changes from 100 $S \cdot cm^{-1}$ in Ref. [29] to 600 $S \cdot cm^{-1}$ in Ref. [37].

The temperature dependence of ASR reported in different papers, using different electrolyte materials is shown in Figure 2B for $PrBaCo_2O_{5+\delta}$. Even considering the most promising results, $PrBaCo_2O_{5+\delta}$ presents ASR values not perfectly suited for cathodic application at temperatures below 600 °C. However, it was found that perovskites performance can be enhanced by Sr doping on Ba site [46], [42], [51]. The typical Sr-doped compound synthesized present half of the barium substituted with strontium ($PrBa_{0.5}Sr_{0.5}Co_2O_{5+\delta}$). The electrochemical parameters and their temperature dependence for this materials are reported in figure 2C and 2D. The enhancement of the conductivity it's noticeable: at 600 °C conductivities are enhanced from the range 150÷900 $S \cdot cm^{-1}$ without Sr doping up to 600÷1400 $S \cdot cm^{-1}$ for doped materials. A similar trend is obtained analyzing the ASR that at 600 °C improves from 0.1÷13 $\Omega \cdot cm^2$ to 0.05÷1 $\Omega \cdot cm^2$.

Considering the ASRs reported in literature, the most promising Pr-based perovskite series are $PrBa_{0.5}Sr_{0.5}Co_{2-x}Fe_xO_{5+\delta}$, synthesized by Choi at al. [45], and $PrBa_{1-x}Sr_xCo_2O_{5+\delta}$, produced by Park at al. [42]. Park's compounds also present the highest conductivity values in Pr-based perovskites literature, but is well known that these materials result unsuitable for cathodic application with the common electrolytes, due to their much higher TEC value. Unfortunately Park et al. do not report in their paper any measurement of thermal expansion coefficient of these promising materials, but a large discrepancy with the TEC of similar materials is not likely.

4.2. Nd-based double perovskites

Considering Nd as A site rare earth for perovskites, the number of publications containing electrochemical characterization is slightly lower than Pr-based ones. The $NdBaCo_2O_{5+\delta}$

conductivity values at 600 °C range from 200 to 1000 $S \cdot cm^{-1}$ (Figure 3A) while ASR values vary from 0.2 to 6 $\Omega \cdot cm^2$ at 600 °C, and by up to two order of magnitudes at 500 °C (figure 3B). In Figure 3C and 3D are reported the electrochemical parameters of $NdBa_{0.5}Sr_{0.5}Co_2O_{5+\delta}$ perovskites. In analogy with what reported for Pr-based ones, the conductivities and ASRs are much improved from the respective undoped perovskites. In fact, conductivity values are found in the range of 300÷2400 $S \cdot cm^{-1}$, while ASR ones between 0.1 and 1.2 $\Omega \cdot cm^2$. The best performing Nd-based perovskite materials have been synthesized by Yoo et al. [55] with $NdBa_{1-x}Sr_xCo_2O_{5+\delta}$ perovskite series. These compounds show the lowest ASR values in Nd-based double perovskite literature and some of the highest conductivity ones.

4.3. Gd-based double perovskites

Compounds containing Gd as A site element were investigated in a large number of papers, mainly as the parent $GdBaCo_2O_{5+\delta}$ double perovskite. However, this material seems to be less efficient than previously discussed ones. Conductivity at 600 °C is reported between 100÷500 $S \cdot cm^{-1}$ (Figure 4A), while ASR (Figure 4B) ranges from 0.3 to 22 $\Omega \cdot cm^2$. A great improvement has been achieved with the substitution of Sr, but only few researchers (Ref. [47] and [73]) investigated the electrochemical properties of this compound, as can be seen in Figure 4C and 4D, reporting conductivity and ASR temperature dependence.

4.4. Sm-based double perovskites

Sm-based materials are less investigated, but some interesting results were reported. As an example, at 600 °C the measured conductivities range between 250 and 850 $S \cdot cm^{-1}$, while ASR values from 0.2 to 15 $\Omega \cdot cm^2$, as can be seen in figure 5A and 5B respectively for $SmBaCo_2O_{5+\delta}$. Only few

papers report a characterization of doped double perovskites with Sm, and in figure 5C and 5D the conductivity and ASRs are shown for $SmBa_{0.5}Sr_{0.5}Co_2O_{5+\delta}$ compounds. Comparing number of publications about Sm with Pr or Nd ones, appears clear that the interest of researchers has been focused on the elements presented above, and it appears that some efforts could still devoted to a further improvement of $SmBaCo_2O_{5+\delta}$ derivate compounds.

5. Doping strategies in double perovskites

The effect of doping on double perovskite materials can be different, depending on the site where the substitution takes place and of course on the parent compound; by the way, some similarities between the effects of the same doping strategy on different compounds can be mentioned.

5.1. A site doping

The most common doping is the substitution of Ba in A' site with Sr. As underlined in the previous sections, Sr doping mainly enhance electrochemical performance of double perovskite material (se Figures 2-5). Both electrical parameters of interest give a positive feedback for materials series with increasing Sr doping content. As can be inferred by the curves reported in Figure 6A-D, for almost every compound series, the electrical conductivity increases with increasing Sr concentration, in the whole temperature range. The maximum of conductivity is often reached with complete substitution of Ba with Sr, but at the same time this usually causes a significant worsening in the oxygen reduction reaction kinetics, as revealed by the measured ASRs: Figure 6E-F shows the dependence of ASR from Sr doping content at different temperatures. The lowest ASR values are found for those compounds with the strontium content $x \geq 0.5$, except for the point with $x = 1$ (i.e. compounds where Ba is completely replaced by Sr) in every series characterized. Indeed at $x = 1$ the ASR sharply increases at every temperature. The main drawback related to Sr doping is the slight increase of TEC values. Unfortunately, most of the authors that investigated Sr-doped double

perovskites series do not report any thermal expansion measurement, except for the paper by Kim et al. [67]. Table 15 report the TEC values of $GdBa_{1-x}Sr_xCo_2O_{5+\delta}$ compounds ($0.0 < x < 1.0$) at different temperature ranges. However, even the lowest TEC value for these materials is still higher than the ideal one, 12-14 10^6 K^{-1}, the commercial electrolyte TEC range. In addition, Gd-based compounds present the lowest average TEC values among all rare earths. In fact, considering only double perovskites with Gd as rare earth in A site, the TEC values present in literature show an average value of 17.9 10^6 K^{-1}.

For what regards the compounds bearing other elements in A site, average TEC increases for Y, Nd, Sm and Pr, presenting respectively 18.8, 19.6, 19.7 and 20.6 10^6 K^{-1}.

Table 14: TECs of selected compounds as a function of Sr content

$GdBa_{1-x}Sr_xCo_2O_{5+\delta}$ [67]	**TEC [10^6 K^{-1}] 80-900°C**
x = 0.0	16.6
x = 0.2	18.0
x = 0.4	18.3
x = 0.6	19.5
x = 1.0	18.8

5.2. B site doping

5.2.1. Iron doping

A common doping element in B site is Fe, used to replace Co in B site. This substitution is realized with the purpose of reducing TEC values in Co based double perovskite materials, since Fe produces stronger bonds with oxygen compared to Co-O ones [56].

Many publications report a Fe doped double perovskites series of materials for cathodic application, mostly resulting in a decrease of electrochemical performance, but also a reduction of TEC value. However, *RE*$BaCo_{2-y}Fe_yO_{5+\delta}$ series of compounds do not even satisfy the TEC requirement for cathodic application, since TEC deceases too slightly with Fe content. Kim et al. [56] presented a publication containing the thermic characterization of $NdBaCo_{2-y}Fe_yO_{5+\delta}$ (with y = 0, 0.5, 1, 1.5, 2) and $GdBaCo_{2-y}Fe_yO_{5+\delta}$ (with y = 0, 0.5, 1) series, resulting in a decrease of TEC values respectively from 21.5 to 18.3 10^6 K^{-1} and from 19.9 to 18.8 10^6 K^{-1}. Zhao et al. [39] achieved a better TEC reduction on $PrBaCo_{2-y}Fe_yO_{5+\delta}$ (with y = 0, 0.5, 1, 1.5, 2) series, reporting a maximum TEC value for y = 0.5 compound, equal to 26 10^6 K^{-1}, while a minimum of 17.2 10^6 K^{-1}, for y = 2 material. However, these slight TEC reductions do not compensate the significant drop in performance related to the replacement of Co with Fe. As is shown in Figure 7A-D, conductivity decrease monotonically with Fe content for almost every series reported. The only exception is represented by Zou et al. [41] compounds, $PrBaCo_{2-y}Fe_yO_{5+\delta}$, that present a structural change from tetragonal to cubic for materials with greater Fe amount than 0.4. This variation of structure leads to a more symmetrical lattice cell, hence a consequent increase in electrical conductivity. Of particular interest is that the dependence of ASR from Fe content (Figure 7E-H) presents the minimum value for the same material, $PrBaCo_{1.6}Fe_{0.4}O_{5+\delta}$. Zou et al. paper is the only one reporting a more detailed characterization of Fe doping double perovskites in the stoichiometric range between 0 and 1. However, the other two Fe-doped series seem to confirm the positive decrease of ASR for the compounds with 0.5 Fe content, but do not present neither cubic structure nor conductivity improvement. Anyway the Nd-based series proposed by Kim at el. [56] present the structure transition from tetragonal to cubic for $y \geq 1.5$ materials. Another investigation of Fe substitution on B site of Pr-based double perovskite is proposed by Yoo et al. [115]. In this paper the oxygen fluxes have been measured through membranes made by $PrBaCo_{2-y}Fe_yO_{5+\delta}$ (with y = 0, 0.2, 0.5, 1, 1.5, 2), resulting in an overall decrease of the specific oxygen flux with Fe content. In this paper, the

transition from tetragonal to cubic structure is reported only for the perovskite with y = 1 and y = 1.5 as Fe content.

Also the influence of other elements have been investigated as B site dopants, especially transition metals such as Ni [50, 51, 71, 116], Cu [24, 117] and Mn [58]. Moreover, some authors reported also a Sc substituted compound [38].

5.2.2. Ni doping

One of the most common element used to dope double perovskites on B site is Ni. In literature characterizations about double perovskites doped with Ni are present for several rare earths on A site. Although B site doping is mainly made to achieve a reduction of TEC values, the electrochemical performance cannot be ignored. In fact, Ni doping leads to considerable improvements of thermal expansion behavior but, regarding conductivity and ASR, higher doping levels cause a drop in electrochemical performance. However, the substitution of a small amount of Ni (y = 0.2-0.4) for Co leads to slightly improved performance and significant TEC reduction, as demonstrated by compounds synthesized by Kim et al. [116]. In this paper, the most promising compound is $NdBaCo_{1.6}Ni_{0.4}O_{5+\delta}$ that presents a TEC value of 16.9 10^6 K^{-1}, lower than the parent compound. Even lower TEC values are achieved with $SmBaCo_{1.6}Ni_{0.4}O_{5+\delta}$ produced by Che at al. [50] and with $GdBaCo_{1.7}Ni_{0.3}O_{5+\delta}$ by Wei at al. [71], that obtained TEC respectively equal to 16.6 and 15.5 10^6 K^{-1}. It is of particular interest that the Ni substitution increases the activation energy of the polarization resistance [116] and conductivity [51] of the cathodes, resulting in better performance in the intermediate temperature range.

5.2.3. Cu doping

An alternative to Fe doping is using Cu to substitute Co in B site of double perovskite, in order to achieve the best tradeoff between TEC and electrochemical performance. TEC values decrease monotonically with increasing Cu content up to y = 1. Several publications report a characterization of compounds with half Co substituted with Cu, leading to the conclusion that TEC is greatly reduced, but also the electrochemical parameters [31, 43, 72]. However, Zhang et al. [24] and Kim et al. [117] investigated more deeply on Cu content, synthesizing material series with increasing Cu content, $YBaCo_{2-y}Cu_yO_{5+\delta}$ (with y = 0, 0.2, 0.4, 0.6, 0.8) and $LnBaCo_{2-y}Cu_yO_{5+\delta}$ (with Ln = Gd and Nd and y = 0, 0.25, 0.5, 0.75, 1) respectively. Zhang et al. report the lowest ASR values (0.125 $\Omega \cdot cm^2$ at 700 °C), among his doped materials for $YBaCo_{1.4}Cu_{0.6}O_{5+\delta}$ compound, and a very low TEC, equal to 14.7 10^6 K^{-1}. The TEC is even lower for y = 0.8 compound, but both present conductivity values below 100 $S \cdot cm^{-1}$ in the intermediate temperature range (500-800 °C), not completely satisfying the requirements of a cathodic application. Similar trend is reported for material series produced and characterized by Kim et al.. TEC values are lowered by Cu content, and $NdBaCo_{1.25}Cu_{0.75}O_{5+\delta}$ (presenting TEC equal to 16.4 10^6 K^{-1}) and $GdBaCoCuO_{5+\delta}$ (TEC equal to 14.5 10^6 K^{-1}) samples show improved cathode performances compared to the Cu-free samples, considering maximum power density obtained in a complete cell. However, the measurements of conductivity and ASR show worsened values with increasing Cu content [117].

5.2.4. Sc doping

Of particular interest is a paper published by Li et al. [38], reporting the substitution of Co with Sc, in order to both reduce TEC and improve performance. This series of materials, $PrBaCo_{2-y}Sc_yO_{5+\delta}$ (with y = 0.05, 0.1, 0.2, 0.5), show that Sc doping leads to a decrease in both ASR and activation

energies, and to a reduction of TEC values (from 23.6 for y = 0.05 to 19.8 10^6 K^{-1} for y = 0.5). However, conductivity values decrease in a significant extent with increasing Sc content, reaching values below 50 $S \cdot cm^{-1}$ for $PrBaCo_{1.5}Sc_{0.5}O_{5+\delta}$. Despite these low conductivity values, Sc doping seems a promising strategy and deserves a deeper investigation, in order to clarify the enhancement of oxygen reduction reaction kinetics at high Sc content.

5.2.5. Mn doping

Using Mn as B site dopant resulted in one of the lowest TEC reported in literature for double perovskite materials containing Co [58]. Kim et al. prepared and characterized a series of $PrBa_{0.5}Sr_{0.5}Co_{2-y}Mn_yO_{5+\delta}$ compounds (y = 0, 0.25, 0.5), obtaining a TEC value of 14.3 10^6 K^{-1} for $PrBa_{0.5}Sr_{0.5}Co_{1.5}Mn_{0.5}O_{5+\delta}$. Although Mn doping reduces electrochemical parameters, at 600 °C the material with y = 0.5 maintains acceptable conductivity and ASR values for cathodic application: 717 $S \cdot cm^{-1}$ and 0.156 $\Omega \cdot cm^2$ respectively. In addition, this study shows also the possibility of producing composite cathodes mixing a cathodic material with an electrolyte one. A cathode made by mixing GDC and $PrBa_{0.5}Sr_{0.5}Co_{1.5}Mn_{0.5}O_{5+\delta}$ in a 50% weight ratio presents a TEC value equal to 11.7 10^6 K^{-1}, a number that completely matches with pure GDC electrolyte TEC (11.4 to 12.5 10^6 K^{-1}, depending on composition).

5.3. Latest developments: Vacancy doping of double perovskites

A very recent trend used to tailor electrochemical performance of double perovskite materials is to produce compounds with a deficient stoichiometry for element on A or A' site. A' site under-stoichiometry was first investigated: a small Ba deficiency (x = 0 ÷ 0.08) in $PrBa_{1-x}Co_2O_{5+\delta}$ caused a shrinkage of the crystal cell size, slightly affected the thermal expansion coefficient, and affected

both the electrical conductivity the electrochemical activity. In details, the electrical conductivity decreased at x = 0.03, then increased at x = 0.05 and again up to x = 0.08, where it was higher than in the stoichiometric compound [86]. The electrochemical activity (as estimated by the ASR measurements) improved with the increasing of barium deficiency up to x = 0.08 and the activation energy decreased accordingly. Afterwards, the same series of materials have been produced by Wang et al. [118], reporting contrasting results. The main difference between those compounds is the synthesis method: Wang et al. synthesized the materials through a Solid State Reaction, while Pang et al. used EDTA-citrate complexing sol-gel method.

The preparation route can strongly influence results due to grain dimension, deposition technique and calcination treatment. The main divergence resulted in conductivity values that, in the temperature range from 600 to 700 °C, vary from 250-300 $S \cdot cm^{-1}$ [86] up to values much higher than 800 $S \cdot cm^{-1}$ for Wang et al.'s compounds. However, considering ASR, Pang et al.'s materials presented slightly higher values, but still reasonably comparable and suitable for cathodic application (0.093 $\Omega \cdot cm^2$ at 600 °C for x = 0.08 while 0.042 $\Omega \cdot cm^2$ for x = 0.06 compound). Anyway, both these publications aroused interest in the A' site deficiency, that seems to be a worthwhile alternative to enhance double perovskites electrochemical performance. The best results among the series produced have been achieved by Pang et al. with $PrBa_{0.92}Co_2O_{5+\delta}$ and by Wang et al. with $PrBa_{0.94}Co_2O_{5+\delta}$. A similar study was performed on $LaBa_{1-x}Co_2O_{5+\delta}$ [119]; this compound tolerated a larger under-stoichiometry (x = 0 ÷ 0.15) without significant modification of the lattice parameters; however, even if ASR values monotonically improved by increasing the deficiency up to 10%, the electrical conductivity decreased drastically with Ba deficiency.

Improvement of the electrochemical activity was also found in $NdBa_{1-x}Co_2O_{5+\delta}$ (x = 0, 0.05, 0.10) [120]; the maximum accepted Ba deficiency is slightly lower than 10%. The Ba deficiency affects the cell dimensions by reduction of the b lattice parameter, and by decrease of the mean oxidation state of Co and increase of the oxygen vacancies. Although the highest total electrical conductivity

is met at a Ba deficiency equal to 5% (750 $S \cdot cm^{-1}$ at 700°C), ASR investigation revealed that the optimal electrocatalytic activity in the oxygen reduction process was realized by the compound with 10% Ba understoichiometry (0.1 $\Omega \cdot cm^2$ at 700°C). The same trends have been observed in the circumstance of an A site deficiency series of double perovskites ($Sm_{1-x}BaCo_2O_{5+\delta}$ with x = 0 ÷ 0.08 [63]). These materials present a decrease in both conductivity and ASR values with increasing deficiency up to x = 0.05; this change in performance is accompanied by an growth in the size of the orthorhombic cell.

The results of these paper about deficient materials could all be rationalized by the interplay between the dominant charge compensation mechanism, as already mentioned in Section 4 for doping elements. The introduction of deficiency generates metal ion vacancies, v''_{Ba} or v''_{RE}, that can be compensated by the generation of new electronic ($Co^{\bullet}_{Co}$) or ionic ($v^{\bullet\bullet}_{O}$) defects, that act as the charge carriers of electrons and ions. A similar effect can be found by changing the A:A' ratio, while keeping the total occupancy of the two sites full, as in $Pr_{1+x}Ba_{1-x}Co_2O_{5+\delta}$ (x = 0 ÷ 0.30): the most interesting result is the decrease of both the cathodic polarization resistance and the thermal expansion coefficient by increasing the amount of rare earth [37].

In conclusion, the deficiency seems to generally improve the electrochemical parameters, with different effects based on material structure. In addition, also a slight reduction of TEC has been observed, even if it does not still appear as decisive for application 'as is' in combination with the common electrolytes.

6. Summary

Double perovskite compounds are promising materials for cathodic application, due to their excellent electrochemical properties. However, it's fundamental to accurately investigate the influence of the stoichiometry of the material on its properties, in order to optimize the cell

performance. This work of review proposed a detailed discussion about the general characteristics of a class of cobalt-based double perovskite compounds with general formula *RE*$BaCo_2O_{5+\delta}$, reporting the main chemical, physical thermal and electrochemical parameters available in the literature, with a special focus on electrical conductivity σ, ASR and TEC.

Conductivity values refer to the ability of moving ions and electrons through the lattice structure of the compound. Since these materials present much higher electronic conductivity, it's complicated to analyze the ionic contribute and make a complete comparison. However, a factor that suggests an idea about the ionic conductivity is the number of oxygen vacancies, hence stoichiometric oxygen content. The vacancies inside the structure is a characteristic element of the double perovskites compounds, and can be controlled tailoring the composition and regulating the annealing process. In order to optimize the performance of the cathode in the oxygen reduction reaction, the role of oxygen vacancies is crucial; this can be evaluated by measuring the oxygen content: this should be lower than 6 (i.e. no vacancies), but without reducing it below the material structure limit (as is the case in $YBaCo_2O_{5+\delta}$), or to avoid a detrimental effect on the electronic conductivity. This dependency has been reported to be related to a reduction of the electron hopping pathway along the Co-O-Co bonds. In addition, some authors argue that the more regular the structure and the bonds, the better is the overlapping between the Co and O orbitals, resulting in enhanced electronic conductivity. This is likely the main reason for the conductivity improvement when A' site is partially doped with Sr (see section 5.1): the smaller ionic radius of Sr respect to that of Ba leads usually to Co-O-Co bonds with angles closer to 180°, hence a more regular lattice. Park et al. [42] explain the improvement of the electrochemical performance as a consequence of the transition from orthorhombic to tetragonal structure that is related to a regularization of the lattice.

The main disadvantage of producing materials with Co is interconnected to the ductility of the states of this element. Changing its spin configuration with increasing temperature, leads to very high TEC values for Co based double perovskites. Partially substituting Co with other metals leads

to a slight mitigation of the sharp difference between cathodes and electrolytes TEC. However, this doping leads also to a reduction of the material performance, except for few percentage of dopant concentration. In addition, in order to achieve a suitable TEC value for double perovskites is necessary to remove almost completely the Co in the material, leading to a remarkable drop in electrochemical performance. Even if Co free cathodes would be very attractive from the environmental point of view, there aren't any competitive compounds to be taken into account yet. A feasible solution to TEC issue, in order to improve cell durability, is the production of graded cathodes, to minimize the mismatch at the cathode-electrolyte layer. However, even this branch of research still requires a bigger effort, but may be a future development for SOFC cathode works. In addition, more accurate analyses would allow to understand how the electrochemical performance are related to crystal structure and preparation conditions. In particular, the understanding of the different contributes of both ASR (i.e. oxygen surface exchange, solid-state diffusion, gas-phase diffusion etc.) and conductivity (i.e. electronic and ionic conductivities) measurements would help to explain how the ORR mechanism occurs and how to improve it. Many possibilities are still available to find solutions to actual SOFC technologic issues.

7. Figure Captions

Figure 1. Total electric conductivities (σ [$S \cdot cm^{-1}$], panel A) and ASRs [$\Omega \cdot cm^2$], panel B) of the investigated compounds grouped by A site rare earth, reported split in quartiles.

Figure 2. Electrochemical characteristics of $PrBaCo_2O_{5+\delta}$ - total electrical conductivities σ ([$S \cdot cm^{-1}$], panel A) and ASR ([$\Omega \cdot cm^2$], panel B) - and of $PrBa_{0.5}Sr_{0.5}Co_2O_{5+\delta}$: total electrical conductivities σ ([$S \cdot cm^{-1}$], panel C) and ASR ([$\Omega \cdot cm^2$], panel D). The legends report the electrolyte used for the measurement of ASRs.

Figure 3. Electrochemical characteristics of $NdBaCo_2O_{5+\delta}$ - total electrical conductivities σ ([$S \cdot cm^{-1}$], panel A) and ASR ([$\Omega \cdot cm^2$], panel B) - and of $NdBa_{0.5}Sr_{0.5}Co_2O_{5+\delta}$: total electrical conductivities σ ([$S \cdot cm^{-1}$], panel C) and ASR ([$\Omega \cdot cm^2$], panel D). The legends report the electrolyte used for the measurement of ASRs.

Figure 4. Electrochemical characteristics of $GdBaCo_2O_{5+\delta}$ - total electrical conductivities σ ([$S \cdot cm^{-1}$], panel A) and ASR ([$\Omega \cdot cm^2$], panel B) - and of $GdBa_{0.5}Sr_{0.5}Co_2O_{5+\delta}$: total electrical conductivities σ ([$S \cdot cm^{-1}$], panel C) and ASR ([$\Omega \cdot cm^2$], panel D). The legends report the electrolyte used for the measurement of ASRs.

Figure 5. Electrochemical characteristics of $SmBaCo_2O_{5+\delta}$ - total electrical conductivities σ ([$S \cdot cm^{-1}$], panel A) and ASR ([$\Omega \cdot cm^2$], panel B) - and of $SmBa_{0.5}Sr_{0.5}Co_2O_{5+\delta}$: total electrical conductivities σ ([$S \cdot cm^{-1}$], panel C) and ASR ([$\Omega \cdot cm^2$], panel D). The legends report the electrolyte used for the measurement of ASRs.

Figure 6. Electrochemical characteristics of selected $REBa_{1-x}Sr_xCo_2O_{5+\delta}$ compounds as a function of strontium content x: total electrical conductivities σ ([$S \cdot cm^{-1}$], 400 °C, panel A; 500 °C, panel B; 600 °C, panel C; 700 °C, panel D) and ASR ([$\Omega \cdot cm^2$], 400 °C, panel E; 500 °C, panel F, 600 °C, panel G, 700 °C, panel H)

Figure 7. Electrochemical characteristics of selected $REBaCo_{2-y}Fe_yO_{5+\delta}$ compounds as a function of iron content y: total electrical conductivities σ ([$S \cdot cm^{-1}$], 400 °C, panel A; 500 °C, panel B; 600 °C, panel C; 700 °C, panel D) and ASR ([$\Omega \cdot cm^2$], 550 °C, panel E; 600 °C, panel F, 650 °C, panel G, 700 °C, panel H)

8. Bibliography

[1] V. Kharton, F. Marques, A. Atkinson, Solid State Ionics, 174 (2004) 135-149.

[2] A. Orera, P.R. Slater, Chem. Mater., 22 (2010) 675-690.

[3] K.D. Kreuer, Annual Review of Materials Research, 33 (2003) 333-359.

[4] H.S. Spacil (1970) US Patent 3,503,809. Filed October 30, 1964

[5] J.A. Kilner, M. Burriel, Ann. Rev. Mater. Res., 44 (2014) 365-393.

[6] S. Tao, J.T.S. Irvine, J. Electrochem. Soc., 151 (2004) A252.

[7] S. Tao, P.I. Cowin, R. Lan, Novel anode materials for SOFC, in: Functional materials for sustainable energy applications, Woodhead Publishing, 2012, 445-477.

[8] D. Singh, R. Singh, Journal of Chemical Sciences, 122 (2010) 807-811.

[9] Y. Hu, Y. Bouffanais, L. Almar, A. Morata, A. Tarancon, G. Dezanneau, Int. J. Hydrogen Energy, 38 (2013) 3064-3072.

[10] E.V. Tsipis, V.V. Kharton, J. Solid State Electrochem., 12 (2008) 1367-1391.

[11] E.V. Tsipis, V.V. Kharton, J. Solid State Electrochem., 12 (2007) 1039-1060.

[12] E.V. Tsipis, V.V. Kharton, J. Solid State Electrochem., 15 (2011) 1007-1040.

[13] A. Tarancón, M. Burriel, J. Santiso, S.J. Skinner, J.A. Kilner, J. Mater. Chem., 20 (2010) 3799.

[14] A.A. Taskin, A.N. Lavrov, Y. Ando, Appl. Phys. Lett., 86 (2005) 091910.

[15] N. Dasgupta, R. Krishnamoorthy, K. Thomas Jacob, Mater. Sci. Eng., B90 (2002) 278-286.

[16] K.T. Lee, A. Manthiram, Chem. Mater., 18 (2006) 1621-1626.

[17] A. Manthiram, J.-H. Kim, Y.N. Kim, K.-T. Lee, J. Electroceram., 27 (2011) 93-107.

[18] P.S. Anderson, C.A. Kirk, J. Knudsen, I.M. Reaney, A.R. West, Solid State Sciences, 7 (2005) 1149-1156.

[19] A. Maignan, C. Martin, D. Pelloquin, N. Nguyen, B. Raveau, J. Solid State Chem., 142 (1999) 247-260.

[20] J.H. Kim, A. Manthiram, J. Electrochem. Soc., 155 (2008) B385.

[21] E.L. Rautama, V. Caignaert, P. Boullay, K. Asish Kundu, V. Pralong, M. Karppinen, C. Ritter, B. Raveau, Chem. Mater., 21 (2009) 102-109.

[22] H. Takahashi, F. Munakata, M. Yamanaka, Phys. Rev. B, 57 (1998) 15211- 15218.

[23] J.-H. Kim, Y.N. Kim, Z. Bi, A. Manthiram, M.P. Paranthaman, A. Huq, Solid State Ionics, 253 (2013) 81-87.

[24] Y. Zhang, B. Yu, S. Lü, X. Meng, X. Zhao, Y. Ji, Y. Wang, C. Fu, X. Liu, X. Li, Y. Sui, J. Lang, J. Yang, Electrochim. Acta, 134 (2014) 107-115.

[25] J. Xue, Y. Shen, T. He, J. Power Sources, 196 (2011) 3729-3735.

[26] E. Chavez, M. Mueller, L. Mogni, A. Caneiro, J. Phys.: Conference Series, 167 (2009) 012043.

[27] D. Muñoz-Gil, D. Pérez-Coll, J. Peña-Martínez, S. Garcia-Martín, J. Power Sources, 263 (2014) 90-97.

[28] D. Akahoshi, Y. Ueda, J. Solid State Chem., 156 (2001) 355-363.

[29] K. Zhang, L. Ge, R. Ran, Z. Shao, S. Liu, Acta Mater., 56 (2008) 4876-4889.

[30] R. Pelosato, A. Donazzi, G. Dotelli, C. Cristiani, I. Natali Sora, M. Mariani, J. Eur. Ceram. Soc., 34 (2014) 4257-4272.

[31] Q. Zhou, T. He, Q. He, Y. Ji, Electrochem. Commun., 11 (2009) 80-83.

[32] Q. Zhou, W.C.J. Wei, Y. Guo, D. Jia, Electrochem. Commun., 19 (2012) 36-38.

[33] J.H. Kim, L. Mogni, F. Prado, A. Caneiro, J.A. Alonso, A. Manthiram, J. Electrochem. Soc., 156 (2009) B1376.

[34] F. Jin, Y. Shen, R. Wang, T. He, J. Power Sources, 234 (2013) 244-251.

[35] R.A. Cox-Galhotra, S. McIntosh, Solid State Ionics, 228 (2012) 14-18.

[36] H. Zhao, Y. Zheng, C. Yang, Y. Shen, Z. Du, K. Świerczek, Int. J. Hydrogen Energy, 38 (2013) 16365-16372.

[37] L. Jiang, F. Li, T. Wei, R. Zeng, Y. Huang, Electrochim. Acta, 133 (2014) 364-372.

[38] X. Li, X. Jiang, H. Xu, Q. Xu, L. Jiang, Y. Shi, Q. Zhang, Int. J. Hydrogen Energy, 38 (2013) 12035-12042.

[39] L. Zhao, J. Shen, B. He, F. Chen, C. Xia, Int. J. Hydrogen Energy, 36 (2011) 3658-3665.

[40] W. Wang, T.S. Peh, S.H. Chan, T.S. Zhang, ECS Transactions, 25 (2009) 2277-2281.

[41] J. Zou, J. Park, B. Kwak, H. Yoon, J. Chung, Solid State Ionics, 206 (2012) 112-119.

[42] S. Park, S. Choi, J. Kim, J. Shin, G. Kim, ECS Electrochem. Letters, 1 (2012) F29-F32.

[43] L. Zhao, Q. Nian, B. He, B. Lin, H. Ding, S. Wang, R. Peng, G. Meng, X. Liu, J. Power Sources, 195 (2010) 453-456.

[44] F. Jin, H. Xu, W. Long, Y. Shen, T. He, J. Power Sources, 243 (2013) 10-18.

[45] S. Choi, S. Yoo, J. Kim, S. Park, A. Jun, S. Sengodan, J. Kim, J. Shin, H.Y. Jeong, Y. Choi, G. Kim, M. Liu, Scientific Reports, 3 (2013) 1-6.

[46] S. Lü, G. Long, X. Meng, Y. Ji, B. Lü, H. Zhao, Int. J. Hydrogen Energy, 37 (2012) 5914-5919.

[47] J.H. Kim, M. Cassidy, J.T.S. Irvine, J. Bae, J. Electrochem. Soc., 156 (2009) B682.

[48] A.K. Azad, J.H. Kim, J.T.S. Irvine, J. Power Sources, 196 (2011) 7333-7337.

[49] L. Jiang, T. Wei, R. Zeng, W.-X. Zhang, Y.-H. Huang, J. Power Sources, 232 (2013) 279-285.

[50] X. Che, Y. Shen, H. Li, T. He, J. Power Sources, 222 (2013) 288-293.

[51] L. Liu, R. Guo, S. Wang, Y. Yang, D. Yin, Ceram. Int., 40 (2014) 16393-16398.

[52] J.H. Kim, J.T.S. Irvine, Int. J. Hydrogen Energy, 37 (2012) 5920-5929.

[53] T.V. Aksenova, L.Y. Gavrilova, D.S. Tsvetkov, V.I. Voronin, V.A. Cherepanov, Russ. J. Phys. Chem. A, 85 (2011) 427-432.

[54] T.V. Aksenova, L.Y. Gavrilova, A.A. Yaremchenko, V.A. Cherepanov, V.V. Kharton, Mater. Res. Bull., 45 (2010) 1288-1292.

[55] S. Yoo, S. Choi, J. Kim, J. Shin, G. Kim, Electrochim. Acta, 100 (2013) 44-50.

[56] Y.N. Kim, J.H. Kim, A. Manthiram, J. Power Sources, 195 (2010) 6411-6419.

[57] M. West, A. Manthiram, Int. J. Hydrogen Energy, 38 (2013) 3364-3372.

[58] J. Kim, S. Choi, S. Park, C. Kim, J. Shin, G. Kim, Electrochim. Acta, 112 (2013) 712-718.

[59] F. Jin, L. Li, T. He, J. Power Sources, 273 (2015) 591-599.

[60] A.C. Tomkiewicz, M. Meloni, S. McIntosh, Solid State Ionics, 260 (2014) 55-59.

[61] A. Jun, J. Kim, J. Shin, G. Kim, Int. J. Hydrogen Energy, 37 (2012) 18381-18388.

[62] N.E. Volkova, L.Y. Gavrilova, V.A. Cherepanov, T.V. Aksenova, V.A. Kolotygin, V.V. Kharton, J. Solid State Chem., 204 (2013) 219-223.

[63] X. Jiang, Q. Xu, Y. Shi, X. Li, W. Zhou, H. Xu, Q. Zhang, Int. J. Hydrogen Energy, 39 (2014) 10817-10823.

[64] Y. Wang, X. Zhao, S. Lü, X. Meng, Y. Zhang, B. Yu, X. Li, Y. Sui, J. Yang, C. Fu, Y. Ji, Ceram. Int., 40 (2014) 11343-11350.

[65] J.H. Kim, M. Cassidy, J.T.S. Irvine, J. Bae, Chem. Mater., 22 (2010) 883-892.

[66] K. Zheng, K. Świerczek, J. Bratek, A. Klimkowicz, Solid State Ionics, 262 (2014) 354-358.

[67] J.H. Kim, F. Prado, A. Manthiram, J. Electrochem. Soc., 155 (2008) B1023.

[68] A. Chang, S. Skinner, J. Kilner, Solid State Ionics, 177 (2006) 2009-2011.

[69] A. Tarancón, S.J. Skinner, R.J. Chater, F. Hernández-Ramírez, J.A. Kilner, J. Mater. Chem., 17 (2007) 3175.

[70] L. Mogni, F. Prado, C. Jiménez, A. Caneiro, Solid State Ionics, 240 (2013) 19-28.

[71] B. Wei, Z. Lü, D. Jia, X. Huang, Y. Zhang, W. Su, Int. J. Hydrogen Energy, 35 (2010) 3775-3782.

[72] S.H. Jo, P. Muralidharan, D.K. Kim, Electrochem. Commun., 11 (2009) 2085-2088.

[73] C. Kuroda, K. Zheng, K. Świerczek, Int. J. Hydrogen Energy, 38 (2013) 1027-1038.

[74] J. Kim, A. Jun, J. Shin, G. Kim, J. Stevenson, J. Am. Ceram. Soc., 97 (2013) 651-656.

[75] Q. Zhou, T. Wei, S. Guo, X. Qi, R. Ruan, Y. Li, Y. Wu, Q. Liu, Ceram. Int., 38 (2012) 2899-2903.

[76] F. Meng, T. Xia, J. Wang, Z. Shi, J. Lian, H. Zhao, J.-M. Bassat, J.-C. Grenier, Int. J. Hydrogen Energy, 39 (2014) 4531-4543.

[77] X. Zhang, H. Hao, Q. He, X. Hu, Physica B: Condensed Matter, 394 (2007) 118-121.

[78] A. McKinlay, J. Phys. Chem. C, 111 (2007) 19120-19125.

[79] S. Lü, B. Yu, X. Meng, Y. Zhang, Y. Ji, C. Fu, L. Yang, X. Li, Y. Sui, J. Yang, Ceram. Int., 40 (2014) 14919-14925.

[80] Y.Q. Jia, J. Solid State Chem., 95 (1991) 184-187.

[81] R.D. Shannon, Acta Crystallogr., 32A (1976) 751-767.

[82] B.C.H. Steele, Solid State Ionics, 134 (2000) 3-20.

[83] K.K. Hansen, K.V. Hansen, Solid State Ionics, 178 (2007) 1379-1384.

[84] G.C. Kostogloudis, C. Ftikos, Solid State Ionics, 126 (1999) 143-151.

[85] Z. Liu, L.-z. Cheng, M.-F. Han, J. Power Sources, 196 (2011) 868-871.

[86] S. Pang, X. Jiang, X. Li, Q. Wang, Z. Su, J. Power Sources, 204 (2012) 53-59.

[87] G. Yang, J. Feng, W. Sun, N. Dai, M. Hou, X. Hao, J. Qiao, K. Sun, J. Power Sources, 268 (2014) 771-777.

[88] W. Zhou, R. Ran, Z. Shao, W. Jin, N. Xu, J. Power Sources, 182 (2008) 24-31.

[89] S.B. Adler, Solid State Ionics, 111 (1998) 125-134.

[90] B. Wei, Z. Lü, W. Jiang, X. Zhu, W. Su, Electrochim. Acta, 134 (2014) 136-142.

[91] D. Han, H. Wu, J. Li, S. Wang, Z. Zhan, J. Power Sources, 246 (2014) 409-416.

[92] D. Chen, R. Ran, Z. Shao, J. Power Sources, 195 (2010) 7187-7195.

[93] D. Chen, R. Ran, K. Zhang, J. Wang, Z. Shao, J. Power Sources, 188 (2009) 96-105.

[94] S. Carter, A. Selcuk, R.J. Chater, J. Kajda, J.A. Kilner, B.C.H. Steele, Solid State Ionics, 53-56 (1992) 597-605.

[95] F.A. Kröger, H.J. Vink, Solid State Physics, 3 (1956) 307-435.

[96] J.M. Ralph, C.c. Rossignol, R. Kumar, J. Electrochem. Soc., 150 (2003) A1518.

[97] C. Rossignol, J.M. Ralph, J. Bae, J.T. Vaughey, Solid State Ionics, 175 (2004) 59-61.

[98] A. Tarancon, J. Penamartinez, D. Marrerolopez, A. Morata, J. Ruizmorales, P. Nunez, Solid State Ionics, 179 (2008) 2372-2378.

[99] Q. Zhou, F. Wang, Y. Shen, T. He, J. Power Sources, 195 (2010) 2174-2181.

[100] F. Tietz, Ionics, 5 (1999) 129-139.

[101] W. Zając, K. Świerczek, J. Molenda, J. Power Sources, 173 (2007) 675-680.

[102] S. Park, S. Choi, J. Shin, G. Kim, Electrochim. Acta, 125 (2014) 683-690.

[103] M. Hou, W. Sun, P. Li, J. Feng, G. Yang, J. Qiao, Z. Wang, D. Rooney, J. Feng, K. Sun, J. Power Sources, 272 (2014) 759-765.

[104] J. Xue, Y. Shen, T. He, Int. J. Hydrogen Energy, 36 (2011) 6894-6898.

[105] V. Dusastre, J.A. Kilner, Solid State Ionics, 126 (1999) 163-174.

[106] Y. Leng, S. Chan, Q. Liu, Int. J. Hydrogen Energy, 33 (2008) 3808-3817.

[107] E. Perry-Murray, S.A. Barnett, Solid State Ionics, 143 (2001) 265-273.

[108] P. Costamagna, M. Panizza, G. Cerisola, A. Barbucci, Electrochim. Acta, 47 (2002) 1079-1089.

[109] X.J. Chen, K.A. Khor, S.H. Chan, L.G. Yu, Mater. Sci. Eng., A335 (2002) 246-252.

[110] D. Chen, Z. Lin, H. Zhu, R.J. Kee, J. Power Sources, 191 (2009) 240-252.

[111] P. Costamagna, P. Costa, V. Antonucci, Electrochim. Acta, 43 (1998) 375-394.

[112] V.M. Janardhanan, V. Heuveline, O. Deutschmann, J. Power Sources, 178 (2008) 368-372.

[113] N.S. Tsvetkova, A.Y. Zuev, D.S. Tsvetkov, J. Power Sources, 243 (2013) 403-408.

[114] E. Suard, F. Fauth, V. Caignaert, I. Mirebeau, G. Baldinozzi, Phys. Rev. B, 61 (2000) R11871-R11874.

[115] C.-Y. Yoo, J.H. Joo, H.J. Lee, J.H. Yu, Mater. Lett., 108 (2013) 65-68.

[116] J.H. Kim, A. Manthiram, Electrochim. Acta, 54 (2009) 7551-7557.

[117] Y.N. Kim, A. Manthiram, J. Electrochem. Soc., 158 (2011) B276.

[118] J. Wang, F. Meng, T. Xia, Z. Shi, J. Lian, C. Xu, H. Zhao, J.-M. Bassat, J.-C. Grenier, Int. J. Hydrogen Energy, 39 (2014) 18392-18404.

[119] S.L. Pang, X.N. Jiang, X.N. Li, H.X. Xu, L. Jiang, Q.L. Xu, Y.C. Shi, Q.Y. Zhang, J. Power Sources, 240 (2013) 54-59.

[120] A. Donazzi, R. Pelosato, G. Cordaro, D. Stucchi, C. Cristiani, G. Dotelli, I. Natali Sora, Electrochim. Acta, Unpublished results (2015).

Figure(s)

Click here to download Figure(s): Figures.docx

Figure 1

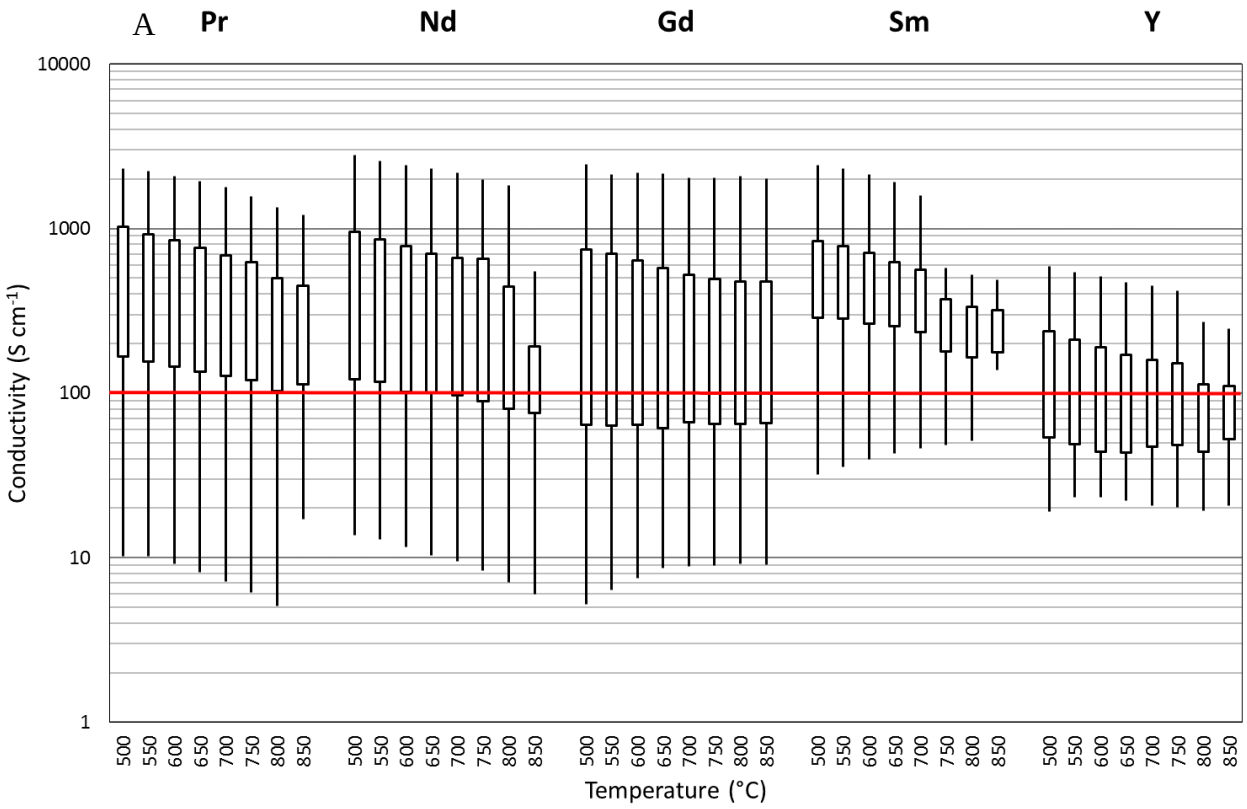

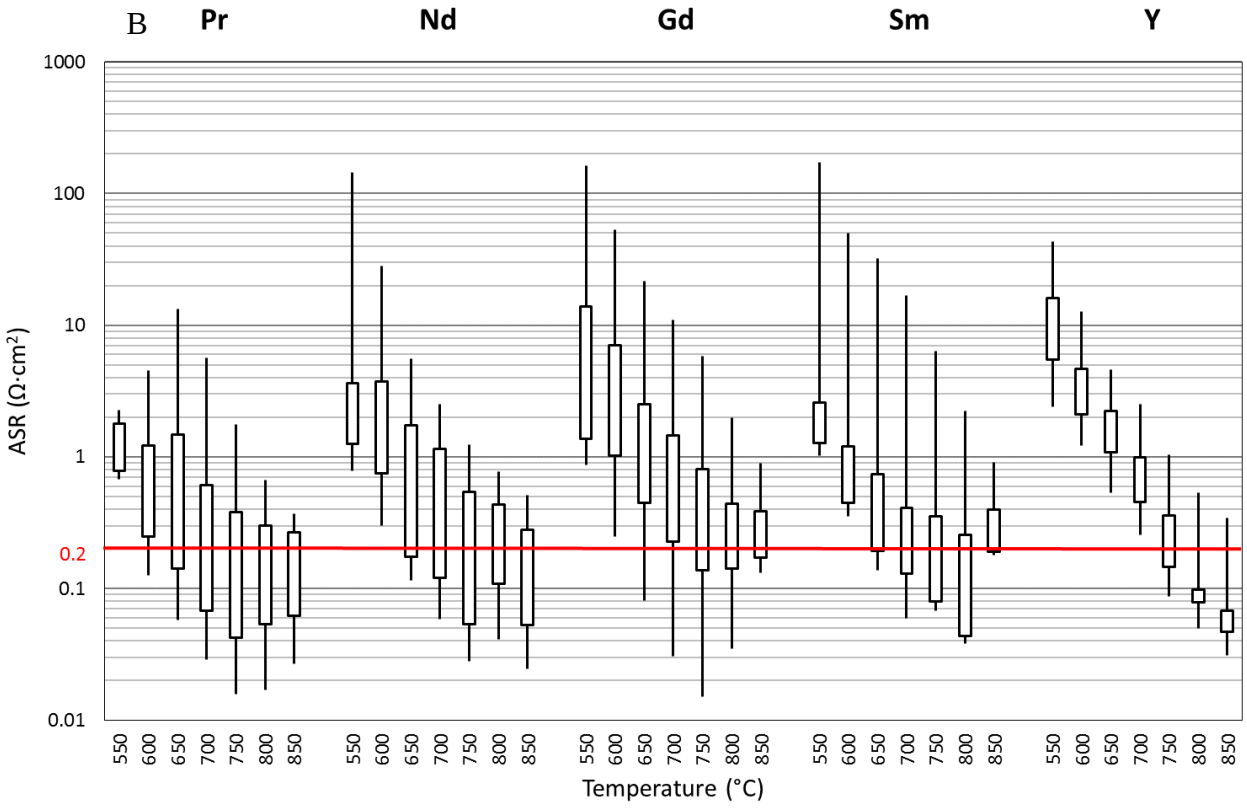

Figure 2

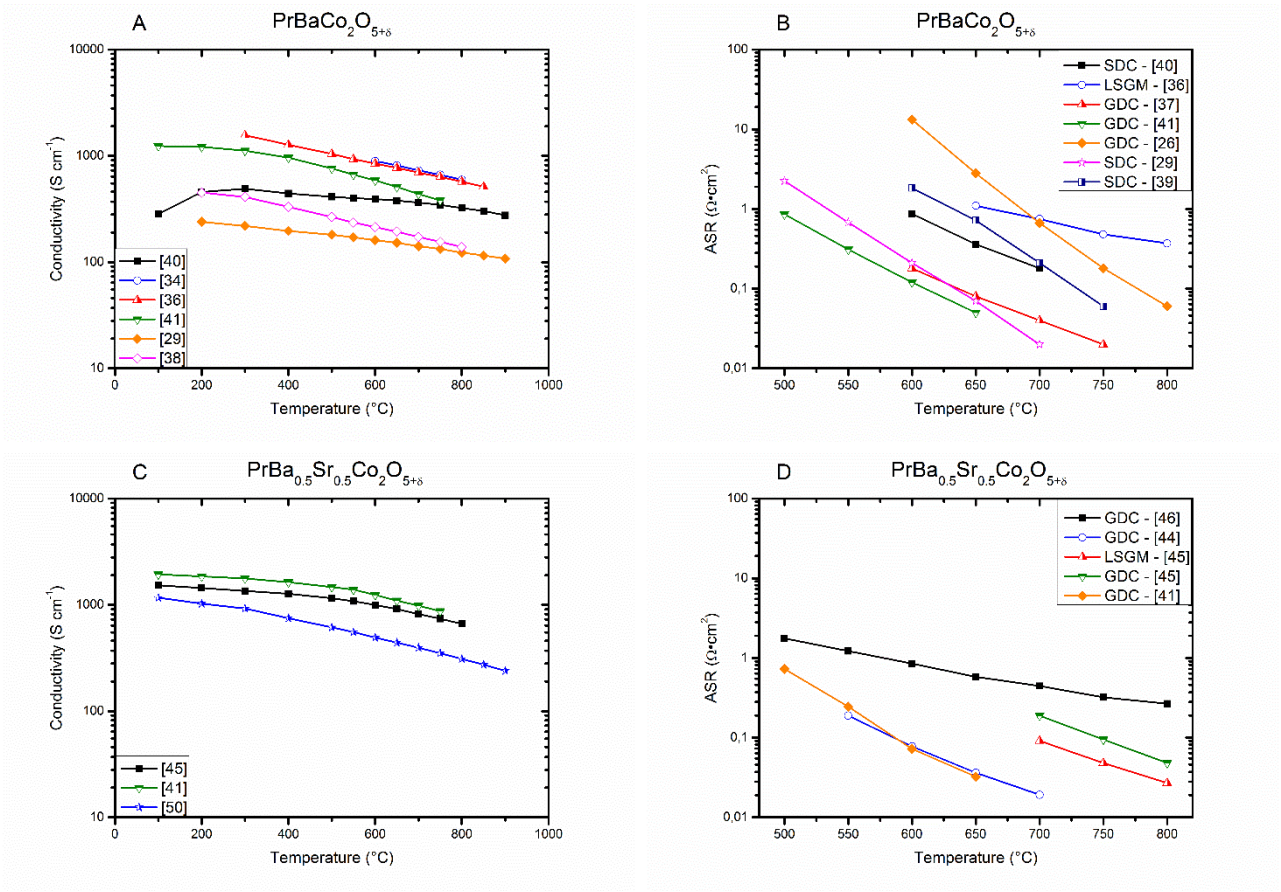
A
PrBaCo2O5+δ
Conductivity (S cm-1)
Temperature (°C)
[40]
[34]
[36]
[41]
[29]
[38]
B
PrBaCo2O5+δ
ASR (Ω•cm2)
Temperature (°C)
SDC - [40]
LSGM - [36]
GDC - [37]
GDC - [41]
GDC - [26]
SDC - [29]
SDC - [39]
C
PrBa0.5Sr0.5Co2O5+δ
Conductivity (S cm-1)
Temperature (°C)
[45]
[41]
[50]
D
PrBa0.5Sr0.5Co2O5+δ
ASR (Ω•cm2)
Temperature (°C)
GDC - [46]
GDC - [44]
LSGM - [45]
GDC - [45]
GDC - [41]

Figure 3

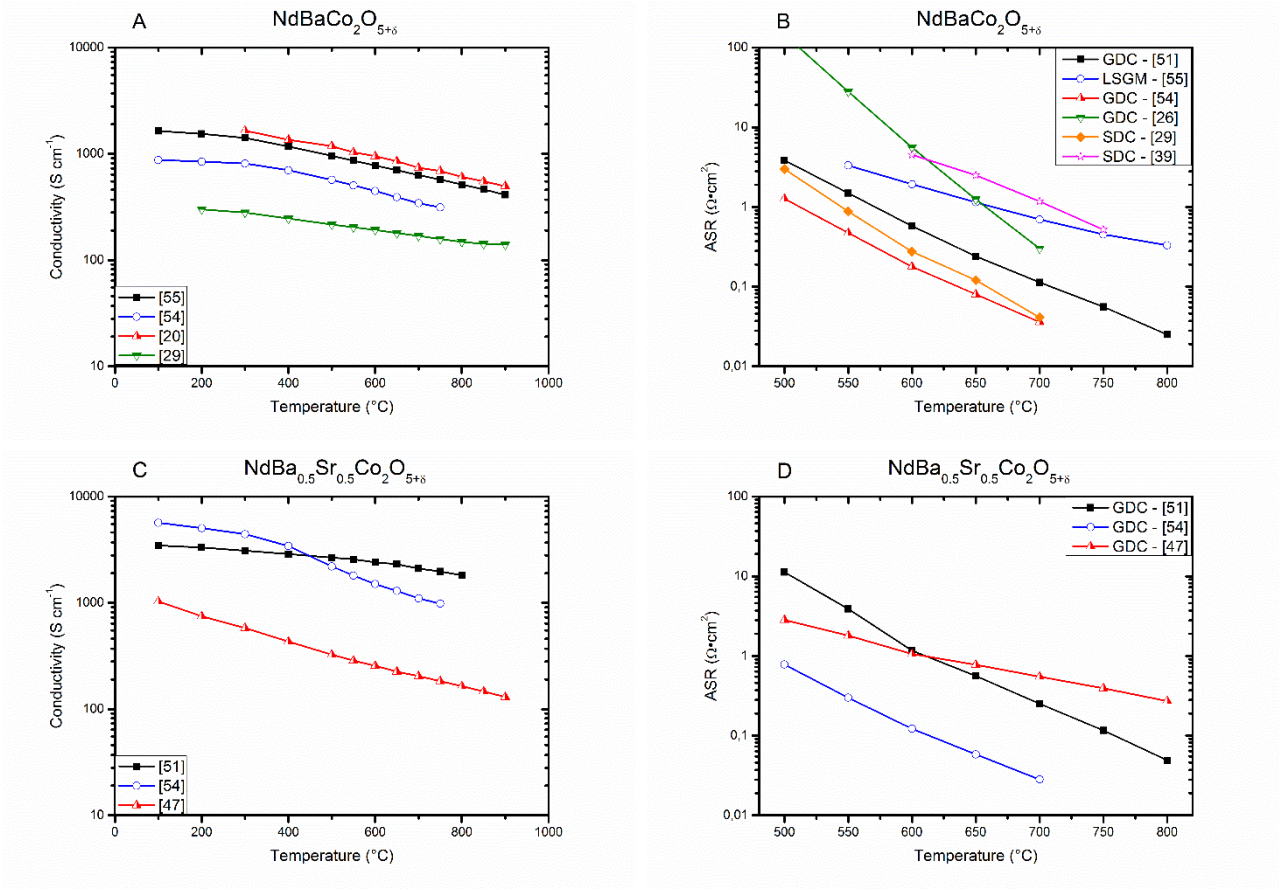
A
NdBaCo2O5+δ
Conductivity (S cm-1)
Temperature (°C)
[55]
[54]
[20]
[29]
B
NdBaCo2O5+δ
ASR (Ω•cm2)
Temperature (°C)
GDC - [51]
LSGM - [55]
GDC - [54]
GDC - [26]
SDC - [29]
SDC - [39]
C
NdBa0.5Sr0.5Co2O5+δ
Conductivity (S cm-1)
Temperature (°C)
[51]
[54]
[47]
D
NdBa0.5Sr0.5Co2O5+δ
ASR (Ω•cm2)
Temperature (°C)
GDC - [51]
GDC - [54]
GDC - [47]

Figure 4

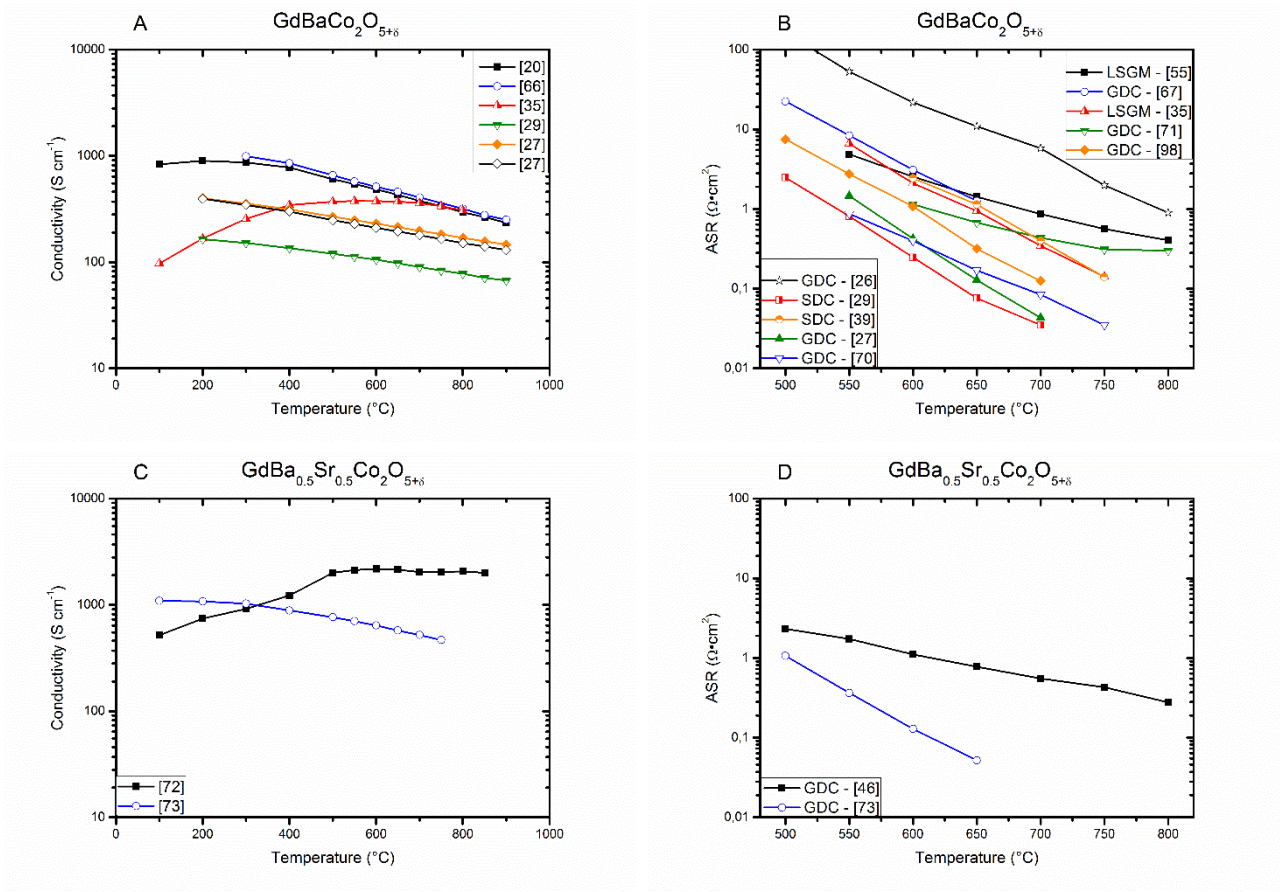
A
GdBaCo2O5+δ
Conductivity (S cm-1)
Temperature (°C)
[20]
[66]
[35]
[29]
[27]
[27]
B
GdBaCo2O5+δ
ASR (Ω•cm2)
Temperature (°C)
LSGM - [55]
GDC - [67]
LSGM - [35]
GDC - [71]
GDC - [98]
GDC - [26]
SDC - [29]
SDC - [39]
GDC - [27]
GDC - [70]
C
GdBa0.5Sr0.5Co2O5+δ
Conductivity (S cm-1)
Temperature (°C)
[72]
[73]
D
GdBa0.5Sr0.5Co2O5+δ
ASR (Ω•cm2)
Temperature (°C)
GDC - [46]
GDC - [73]

Figure 5

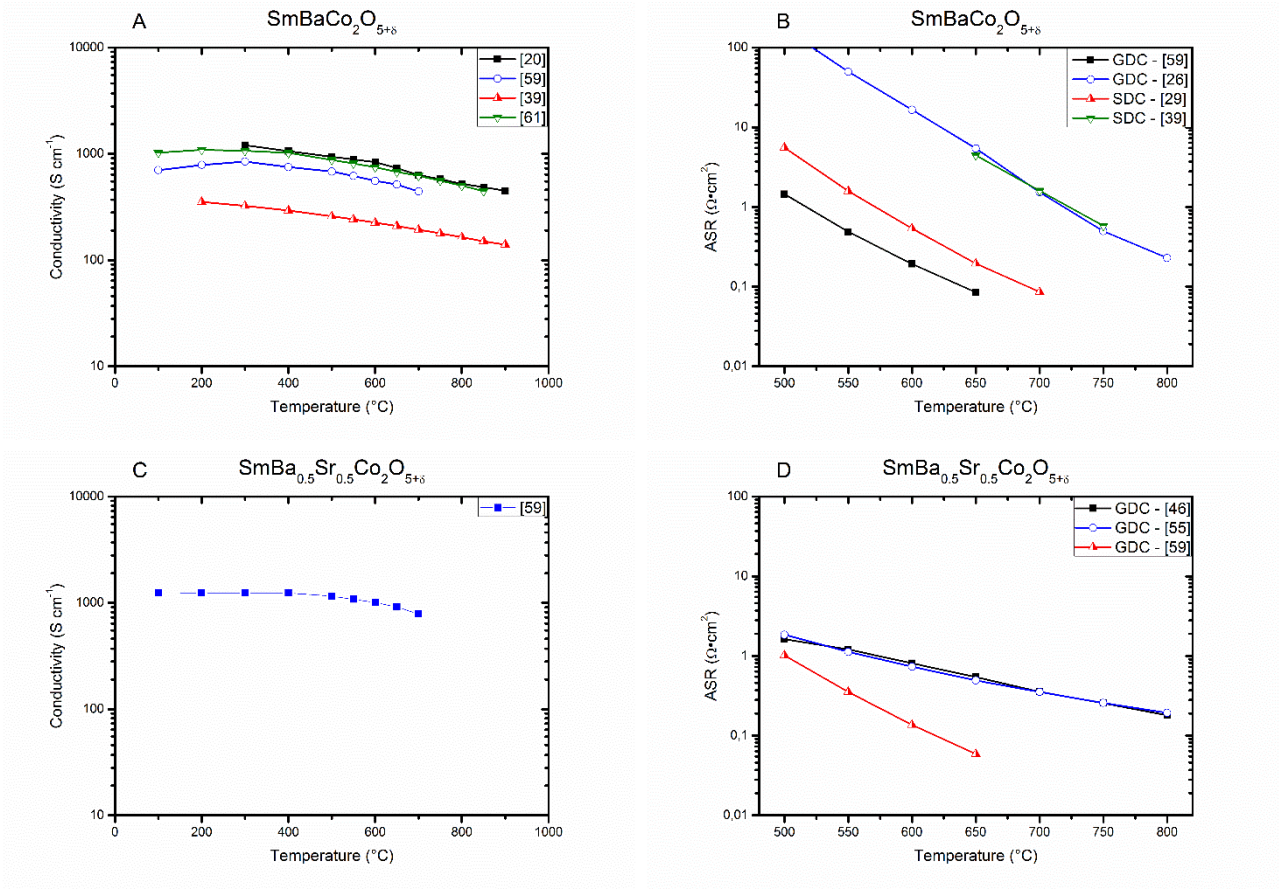
A
SmBaCo2O5+δ
Conductivity (S cm-1)
Temperature (°C)
[20]
[59]
[39]
[61]
B
SmBaCo2O5+δ
ASR (Ω•cm2)
Temperature (°C)
GDC - [59]
GDC - [26]
SDC - [29]
SDC - [39]
C
SmBa0.5Sr0.5Co2O5+δ
Conductivity (S cm-1)
Temperature (°C)
[59]
D
SmBa0.5Sr0.5Co2O5+δ
ASR (Ω•cm2)
Temperature (°C)
GDC - [46]
GDC - [55]
GDC - [59]

Figure 6

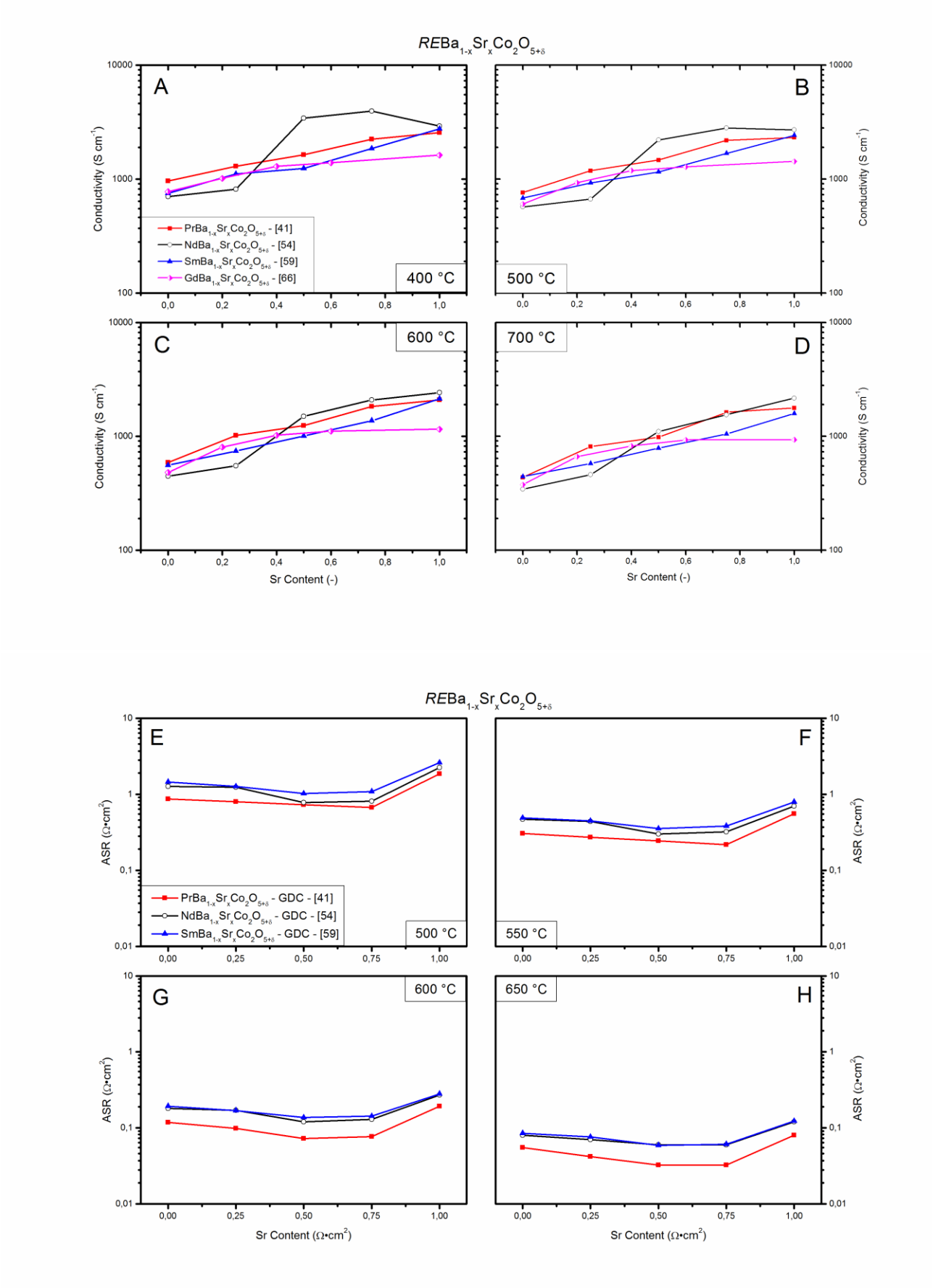
REBa1-xSrxCo2O5+δ
A
B
C
D
400 °C
500 °C
600 °C
700 °C
Conductivity (S cm-1)
Sr Content (-)
PrBa1-xSrxCo2O5+δ - [41]
NdBa1-xSrxCo2O5+δ - [54]
SmBa1-xSrxCo2O5+δ - [59]
GdBa1-xSrxCo2O5+δ - [66]
REBa1-xSrxCo2O5+δ
E
F
G
H
500 °C
550 °C
600 °C
650 °C
ASR (Ω•cm2)
Sr Content (Ω•cm2)
PrBa1-xSrxCo2O5+δ - GDC - [41]
NdBa1-xSrxCo2O5+δ - GDC - [54]
SmBa1-xSrxCo2O5+δ - GDC - [59]

Figure 7

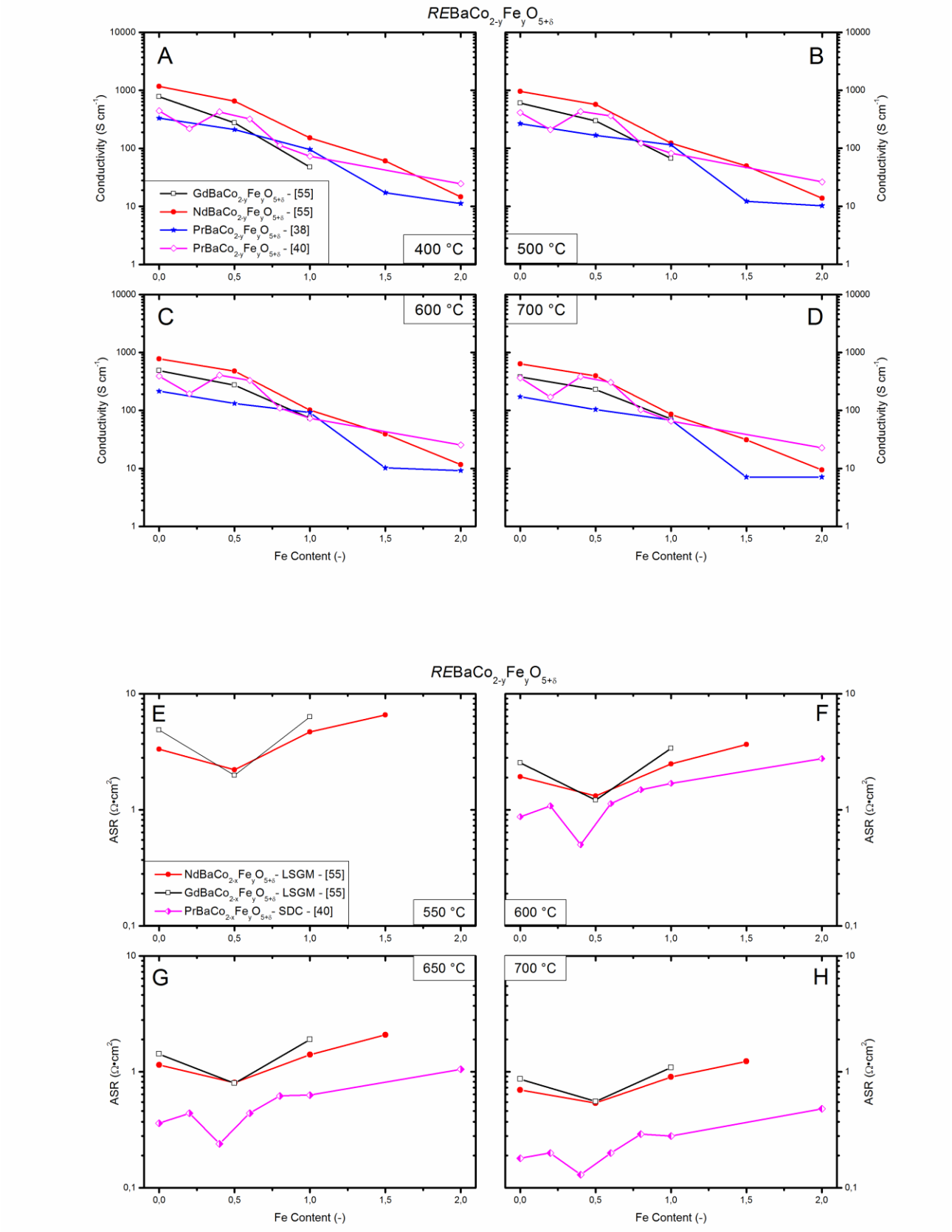
REBaCo2-yFeyO5+δ
A
B
C
D
400 °C
500 °C
600 °C
700 °C
Conductivity (S cm-1)
Fe Content (-)
GdBaCo2-yFeyO5+δ - [55]
NdBaCo2-yFeyO5+δ - [55]
PrBaCo2-yFeyO5+δ - [38]
PrBaCo2-yFeyO5+δ - [40]
REBaCo2-yFeyO5+δ
E
F
G
H
550 °C
600 °C
650 °C
700 °C
ASR (Ω•cm2)
Fe Content (-)
NdBaCo2-xFeyO5+δ - LSGM - [55]
GdBaCo2-xFeyO5+δ - LSGM - [55]
PrBaCo2-xFeyO5+δ - SDC - [40]